Naval Research Laboratory

Washington, DC 20375-5320

Colorimetric Biosensor: Crosslinker Variations

Brandy J. White

Laboratory for the Study of Molecular Interfacial Interactions
Center for Bio/Molecular Science & Engineering

Chris R. Taitt

Laboratory for Biomolecular Dynamics
Center for Bio/Molecular Science & Engineering

Edikan Archibong

Department of Chemical and Biomedical Engineering, University of South Florida
Tampa, FL

Iwona A. Leska

Nova Research, Inc.
Alexandria, VA

October 9, 2018

REPORT DOCUMENTATION PAGE

1. REPORT DATE (DD-MM-YYYY)
09-10-2018

2. REPORT TYPE
Memorandum Report

3. DATES COVERED (From - To)
0/01/2012 - 9/20/2018

4. TITLE AND SUBTITLE

Colorimetric Biosensor: Crosslinker Variations

5a. CONTRACT NUMBER

5b. GRANT NUMBER

5c. PROGRAM ELEMENT NUMBER

6. AUTHOR(S)

Brandy J. White, Chris R. Taitt, Edikan Archibong* and Iwona Leska**

5d. PROJECT NUMBER

5e. TASK NUMBER

5f. WORK UNIT NUMBER
69-6A26

7. PERFORMING ORGANIZATION NAME(S) AND ADDRESS(ES)

Center for Bio/Molecular Science & Engineering
Naval Research Laboratory
4555 Overlook Avenue, SW
Washington, DC 20375-5344

8. PERFORMING ORGANIZATION REPORT NUMBER

NRL/MR/6930--18-9820

9. SPONSORING / MONITORING AGENCY NAME(S) AND ADDRESS(ES)

10. SPONSOR / MONITOR'S ACRONYM(S)

NRL 6.2

11. SPONSOR / MONITOR'S REPORT NUMBER(S)

12. DISTRIBUTION / AVAILABILITY STATEMENT

DISTRIBUTION STATEMENT A: Approved for public release; distribution is unlimited.

13. SUPPLEMENTARY NOTES
*Uninversity of South Florida, **Nova Research, Inc.

14. ABSTRACT

This report is related to an effort that seeks to develop autonomous sensors for environmental monitoring of changes in bacterial populations. The approach uses porphyrin modified antimicrobial peptides to produce colorimetric signatures, enabling the use of devices originally developed for chemical sensing applications. Here, we describe initial work focused on development of the covalent porphyrin-peptide constructs and the evaluation of those materials in the presence and absence of bacterial targets in aqueous solution.

15. SUBJECT TERMS

environmental sensor, biosensor, colorimetric, porphyrin
antimicrobial peptide

16. SECURITY CLASSIFICATION OF:

a. REPORT	b. ABSTRACT	c. THIS PAGE
Unclassified Unlimited	Unclassified Unlimited	Unclassified Unlimited

17. LIMITATION OF ABSTRACT
Unclassified Unlimited

18. NUMBER OF PAGES
43

19a. NAME OF RESPONSIBLE PERSON
Brandy J. White

19b. TELEPHONE NUMBER (include area code)
(202) 404-6100

Standard Form 298 (Rev. 8-98)
Prescribed by ANSI Std. Z39.18

This page intentionally left blank.

CONTENTS

FIGURES

TABLES

EXECUTIVE SUMMARY

In October 2012, the Center for Bio/Molecular Science and Engineering at the Naval Research Laboratory (NRL) began an effort intended to develop porphyrin modified antimicrobial peptides for application to colorimetric detection of bacterial threats. The goal was to apply the spectrophotometric characteristics of porphyrins and/or metalloporphyrins for indication of changes in the conformation of antimicrobial peptides upon interaction with targets. These covalent constructs would be used in an array format, and the relative responses of the materials would be applied to detection and discrimination of bacterial species in environmental air samples. This report addresses a component of the initial indicator development effort, focusing on the linkage between the porphyrin and antimicrobial peptide components.

This page intentionally left blank.

COLORIMETRIC SENSOR: CROSSLINKER VARIATIONS

INTRODUCTION

In October 2012, the Center for Bio/Molecular Science and Engineering at the Naval Research Laboratory (NRL) began an effort intended to develop porphyrin modified antimicrobial peptides for application to colorimetric detection of bacterial threats. The goal was to apply the spectrophotometric characteristics of porphyrins and/or metalloporphyrins for indication of changes in the conformation of antimicrobial peptides upon interaction with targets. These covalent constructions would be used as an array and the relative responses of the materials would be applied to detection and discrimination of bacterial species in environmental air samples. This report addresses a component of the initial indicator development effort, focusing on the linkage between the porphyrin and antimicrobial peptide components.

Antimicrobial peptides (AMPs) are a group of biomolecules that have evolved to recognize and kill target microbes by binding to and disrupting cell membranes (Figure 1). Several unique characteristics of AMPs make them extremely attractive alternatives to antibodies for detection of microbial biothreats: resistance to proteases, stability to environmental extremes, and high affinity, overlapping (but not identical) binding reactions with microbial membranes and membrane components. Arrays of AMPs have been used to detect and classify microbial pathogens with similar or superior sensitivity to antibody-based assays; their broad-spectrum binding activities also provide the potential for detection of unknown (or unsuspected) microbes. [1, 2, 3, 4, 5] In prior reports, the AMP mediated target binding utilized an additional optical "tracer" (e.g., labeled antibody, non-specific dye) for signal transduction. This constraint increases the number of reagents required and the overall complexity of assays. Development of an AMP-based material that is capable of both recognition and signal generation without addition reagents or steps is highly desirable. This type of construct would provide greatly enhanced potential for application of AMP-based detection techniques to autonomous/distributed sensing platforms.
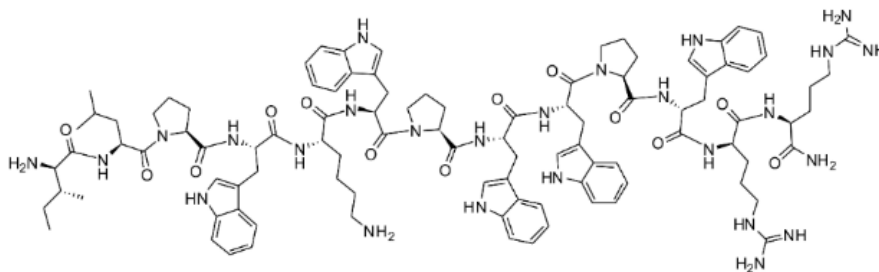
Fig. 1 – Structure of the AMP indolicidin.

Prior reports have described modification of porphyrin structures using single amino acids or dipeptides. [6, 7, 8] Changes in porphyrin fluorescence induced by binding of these constructs to proteins were observed. Our prior work described indicators developed to provide indication of bacterial presence without the need for additional reagents through utilization of changes in porphyrin spectrophotometric characteristics. [9, 10] That work used 1-ethyl-3-(3-dimethylaminopropyl) carbodiimide hydrochloride (EDC) chemistry to link the carboxylic acid group of the porphyrin structure to an amine group on the peptide. Here, we report on variations in performance generated through different linkages (Figure 2) between the porphyrin structure and the peptide as well as through control of the position of the modification within the peptide structure.

Fig. 2 – Crosslinker structures; *N*-(α-maleimidoacetoxy) succinimide ester (AMAS); (*N*-γ-maleimidobutyryl-oxysuccinimide ester) (GMBS); *N*-(ε-maleimidocaproyloxy) succinimide ester (EMCS); *m*-maleimidobenzoyl-*N*-hydroxysuccinimide ester (MBS); succinimidyl 4-(*N*-maleimidomethyl)cyclohexane-1-carboxylate (SMCC).

Table 1. Crosslinkers and properties

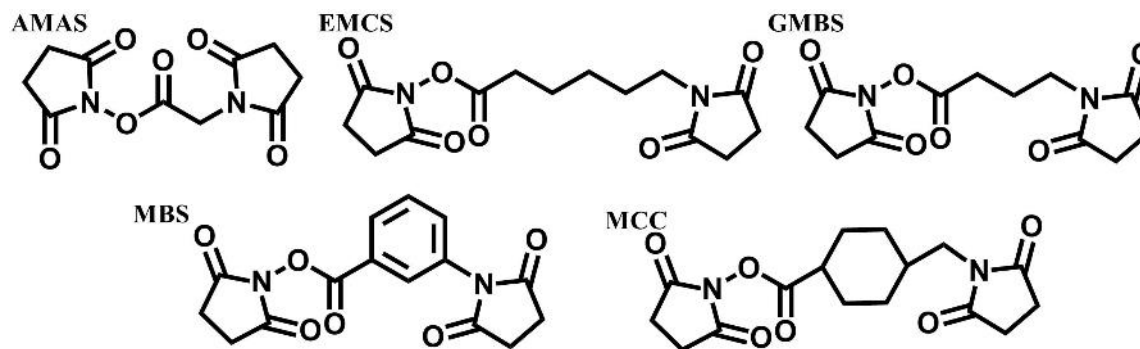|	Crosslinker	MW	Spacer (Å)	CAS
AMAS	*N*-(α-maleimidoacetoxy) succinimide ester	252.2	4.4	55750-61-3
GMBS	(*N*-γ-maleimidobutyryl-oxysuccinimide ester)	280.2	7.3	80307-12-6
EMCS	*N*-(ε-maleimidocaproyloxy)succinimide ester	308.3	9.4	55750-63-5
MBS	*m*-maleimidobenzoyl-*N*-hydroxysuccinimide ester	314.3	7.3	58626-38-3
SMCC	succinimidyl 4-(*N*-maleimidomethyl)cyclohexane-1-carboxylate	334.3	8.3	57757-57-0

METHODS

Meso-tri(4-sulfonatophenyl)mono(4-carboxyphenyl) porphyrin (C_1S_3TPP) was obtained from Frontier Scientific (Logan, UT; Figure 3). 1-Ethyl-3-(3-dimethylaminopropyl) carbodiimide hydrochloride (EDC), N-hydroxysuccinimidyl ester (NHS) and sulfo-NHS, all crosslinkers (Table 1) and Immobilized TCEP Disulfide Reducing Gel were purchased from Pierce Thermo Scientific (Rockland, IL). Ethylenediamine was purchased from Alfa Aesar. The antimicrobial peptide (AMP) indolicidin (Indol) was purchased from American Peptide Company (Sunnyvale, CA). Two custom variants of indolicidin ($ILPWKPWWPWRR-NH_2$) were synthesized by BioSynthesis Inc. (Lewisville, TX) and purified to 90% purity. This peptide is unstructured in solution and forms an extended boat conformation on interaction with a bacterial cell. One variant (C1-Indol) was synthesized with an appended N-terminal cysteine while the second variant was synthesized with an appended C-terminal cysteine (C14-Indol).

Fig. 3 – Porphyrin structure: meso-tri(4-sulfonatophenyl)mono(4-carboxyphenyl) porphyrin (C_1S_3TPP).

C_1S_3TPP (MW 986.9) was converted to an amine-terminated variant by treating with a 10 molar excess of ethylenediamine and a four molar excess (each) of EDC and sulfo-NHS in 0.1M MES pH 6. After 3h

incubation, the reaction was placed in a 500 MWCO dialysis bag and dialyzed at 4°C against PBS (20 changes) and then water (2 changes). Contents were then frozen on dry ice and lyophilized.

The amine-terminated porphyrin was then brought up in anhydrous dimethyl sulfoxide (DMSO) and incubated for 3h with 1.1 molar equivalents of linker (Table 1), also brought up in anhydrous DMSO. Separately, C1-Indol and C14 Indol-were treated for 20 min with immobilized TCEP gel to ensure reduction of any disulfide groups and were then diluted to 0.1 mg/mL in PBS. The linker-treated porphyrins and reduced peptides were then mixed at a 1.1:1 stoichiometry and incubated for 2h. The resultant mixes were then dialyzed (2000 MWCO) exhaustively against PBS. Construct concentrations are estimated based on the initial concentration of AMP and the total final volume of the preparation.

Direct covalent attachment of C_1S_3TPP to indolicidin was completed as described previously. [10] Attachment was accomplished under aqueous conditions using carbodiimide-mediated coupling in 50 mM MES buffer pH 6. Stock solutions of C_1S_3TPP, EDC, NHS, and indolicidin were prepared in absolute ethanol prior to mixing. The composition of the reaction mixture (molar equivalents) was 1 peptide: 1 porphyrin: 5 EDC: 5 NHS. After completion of the coupling reaction (>>2 hours), reaction the mixture was diluted with water and dialyzed (2000 molecular weight cutoff) exhaustively against water and phosphate-buffered saline (PBS).

The bacterial targets for binding studies, *Escherichia coli* (XL1 blue) and *Bacillus cereus* (ATCC 10987), were grown to mid-log in Luria (37°C) or tryptic soy broth (30°C), respectively, before harvesting by centrifugation at $2800 \times g$ for 10 min (4°C). Cell pellets were washed twice with phosphate-buffered saline (PBS), pH 7.4 and resuspended in 1/5 original volume of PBS. Cell numbers (in PBS) were then counted by flow cytometry (Accuri C6). Cell suspensions not used immediately were diluted with an equal volume of 60% glycerol in PBS before storage at -20°C. Prior to analysis, cells were diluted in PBS to the appropriate concentrations.

A Tecan XSafire microtiter plate reader was used to measure the absorbance and fluorescence of the porphyrin-AMP constructs in the presence and absence of bacterial targets. Absorbance was measured from 360 to 800 nm in steps of 2 nm. Fluorescence emission spectra were collected from 500 to 800 nm (2 nm steps) using 415 nm excitation while fluorescence excitation spectra were collected from 385 to 619 nm (2 nm steps) at 730 nm emission. In both cases, a gain of 160 was applied with 50 flashes at 400 Hz, and an integration time of 20 µs was employed. All experiments were conducted in 15% DMSO in order to ensure a homogeneous solution; porphyrin-AMP constructs have low water solubility due to the hydrophobicity of the porphyrin utilized and inherent solubilities of the AMPs. Cell concentrations ranging from 10^7 to 10^3 cells/mL were employed. Indicator concentrations were varied from 0.1 to 12 µM. In all cases, difference spectra were calculated as the point-by-point subtraction of indicator only spectra from spectra collected for the indicator in the presence of the target.

Fluorescence spectra for cell pellets utilized a total initial volume of 765 µL with 8 µM indicator and varying target cell concentrations in an Eppendorf tube (1.5 mL). As above, all experiments were conducted in 15% DMSO. The fluorescence of the initial solution was measured before centrifuging at 7,500 rpm for 10 min. Supernatant was then removed (665 µL), and the remaining solution and pellet were mixed thoroughly to resuspend components. The fluorescence of both the resulting supernatant and the resuspended pellet were collected using the microtiter plate protocol described above.

RESULTS

The goal in generation of porphyrin-modified AMPs is to provide an array of constructs capable of detecting bacterial species, in which the AMP components serve as target recognition "domains" while the porphyrin components provide a mechanism of signal generation; specifically, the spectrophotometric characteristics of the porphyrin are impacted by AMP structural changes upon binding of the target. Direct interaction of a porphyrin with the bacterial target may result in changes to the spectrophotometric characteristics, but these will likely be nonspecific. As reported previously, no concentration dependent changes in the spectrophotometric characteristics of the porphyrin were noted upon interaction with either *E. coli* or *B. cereus*. [9, 10]

Figure 3 presents the absorbance and fluorescence spectra for the C_1S_3TPP porphyrin bound to C14-Indol via the five crosslinkers. As shown, the spectrophotometric characteristics of these variants are highly similar. The characteristics are, however, somewhat different from those of the C1-Indol variants (Figure 4). Differences include shoulders on the leading edge of the Soret (420 nm) in the absorbance spectra and the leading edges of the 420 nm peak in the fluorescence excitation spectra. Figure 5 presents these spectra overlaid with the original C_1S_3TPP-Indol synthesized using EDC/NHS chemistry.[10] As shown, the EDC/NHS variant has higher absorbance and fluorescence intensities than the crosslinked variants. This may reflect lower yield in the synthetic process. Alternatively, the nonspecific EDC/NHS construct may incorporate up to two porphyrins per peptide (at the N-terminus and at K5), resulting in higher molar adsorption and fluorescence.
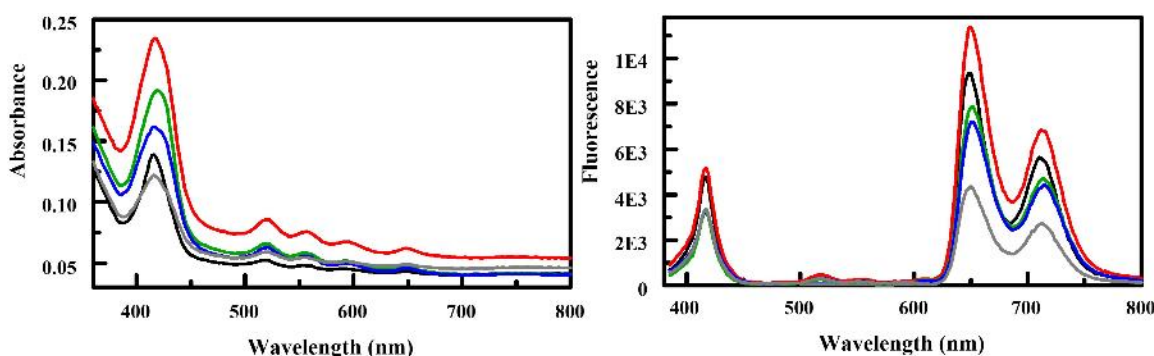

Fig. 4 – Absorbance (left) and fluorescence (right) characteristics for the C14 end C_1S_3TPP modified indolicidin (16 µM): AMAS (black), GMBS (red), EMCS (green), MBS (blue), SMCC (gray).
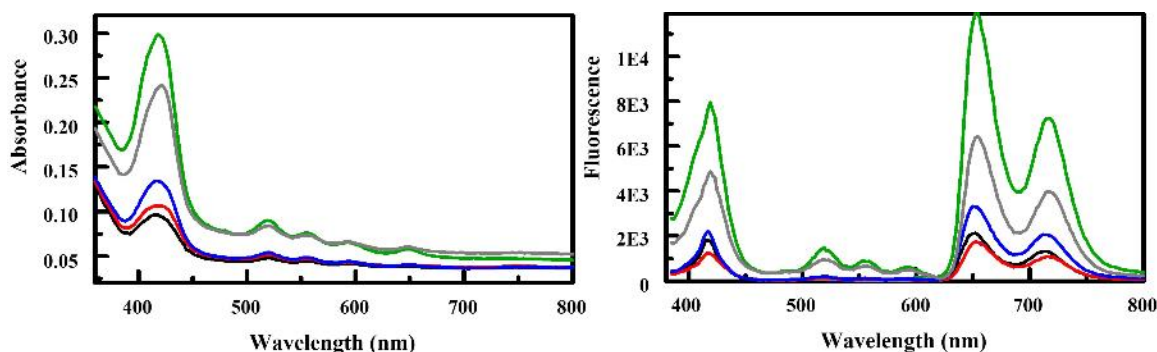

Fig. 5 – Absorbance (left) and fluorescence (right) characteristics for the C1 end C_1S_3TPP modified indolicidin (16 µM): AMAS (black), GMBS (red), EMCS (green), MBS (blue), SMCC (gray).

Fig. 6 – Comparison of EDC/NHS C$_1$S$_3$TPP-Indol (11.8 µM; pink) to the crosslinked constructs of Figures 4 and 5. Absorbance (left) and fluorescence (right) characteristics for the C$_1$S$_3$TPP modified indolicidin (16 µM): AMAS (black), GMBS (red), EMCS (green), MBS (blue), SMCC (gray). Traces include both C1 and C14 variants.
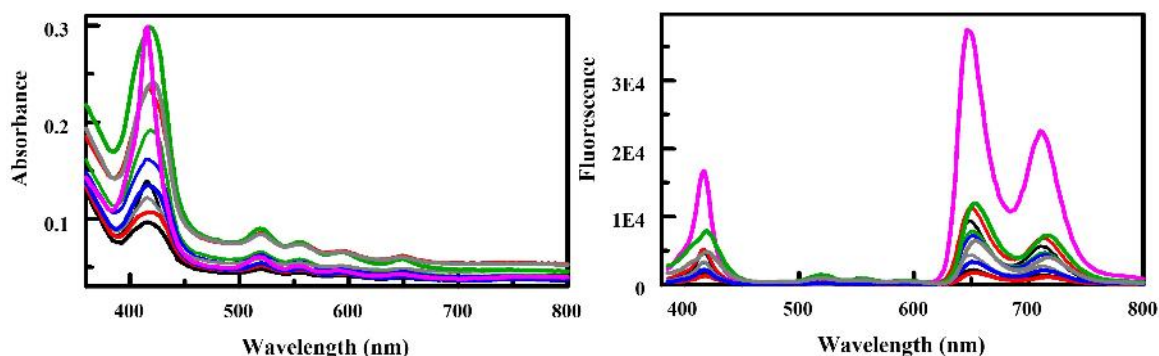
The interaction of the EDC/NHS C$_1$S$_3$TPP-Indol construct with bacterial targets (*E. coli* and *B. cereus*) produced significant and highly similar changes in absorbance (Figure 7; additional data Appendix A). Fluorescence spectra show more noise than expected, but concentration dependent changes were sufficient for analysis (Figure 7). [10] The performance of the EDC/NHS construct will be used as a benchmark for evaluation of the crosslinked constructs in the following sections. The fits (green lines) from this data set (Figure 7) will be included in plots of the concentration dependence for the C1- and C14-Indol materials.
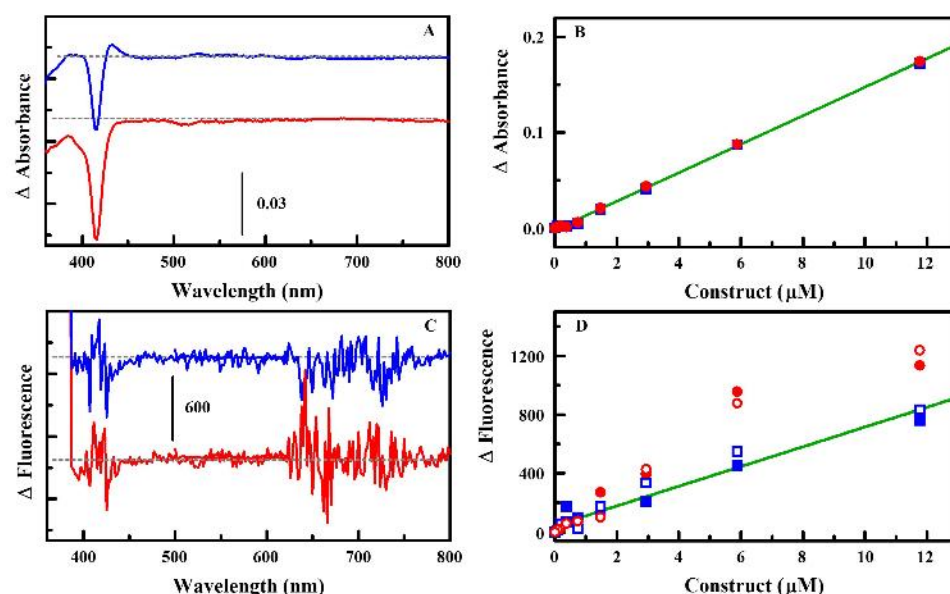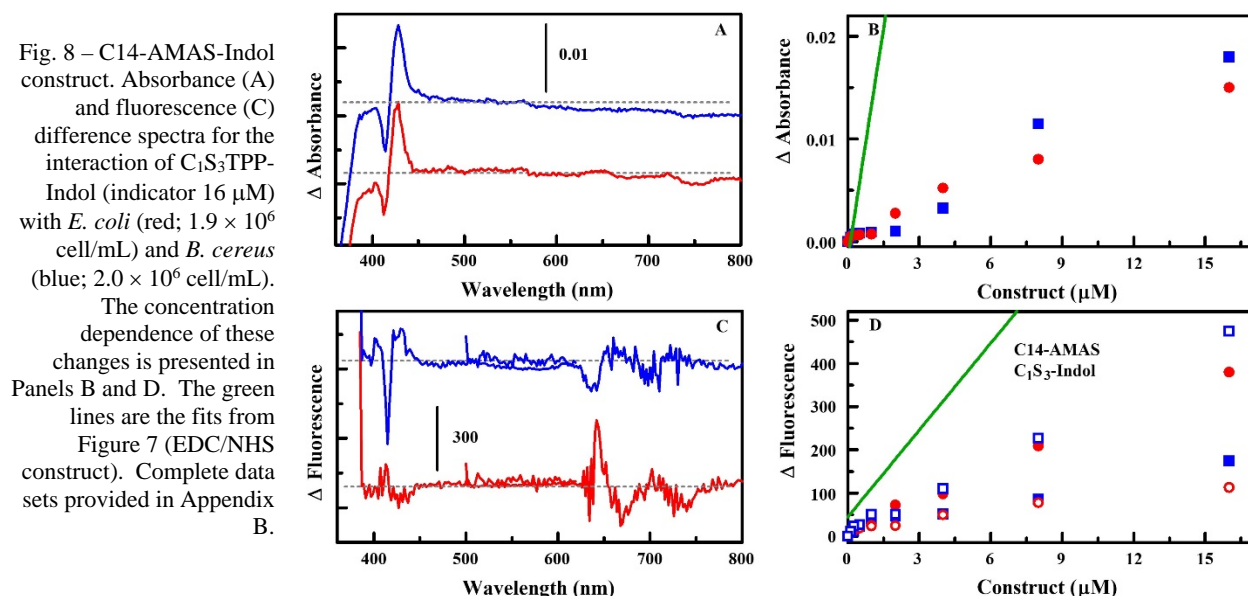

Fig. 7 – EDC/NHS C$_1$S$_3$TPP-Indol construct. Absorbance (A) and fluorescence (C) difference spectra for the interaction of C$_1$S$_3$TPP-Indol (indicator 11.8 µM) with *E. coli* (red; 1.9 × 10^6 cell/mL) and *B. cereus* (blue; 2.0 × 10^6 cell/mL). The concentration dependence of these changes is presented in Panels B and D. Complete data sets provided in Appendix A.

C14-Indol constructs.

The C14-AMAS-Indol construct was evaluated using the approaches described for the EDC/NHS construct; AMAS was the shortest of the linkers used. As shown in Figure 8, changes in the spectrophotometric characteristics of this construct are smaller than those noted for the EDC/NHS construct. In addition, changes in the fluorescence of the construct are different depending on which target is considered. If spectrophotometric changes in the construct result from changes in the AMP structure, as proposed, rather than resulting from direct porphyrin-cell interactions, the peak/trough positions in the difference spectra would be expected to be similar regardless of the type of bacteria evaluated. Affinity could vary between bacterial targets dependent on the properties of the AMP. The differences noted in the

fluorescence difference spectra (Figure 8) tend to indicate at least some interaction of the bacterial target directly with the porphyrin. The minimal changes in absorbance and fluorescence could indicate that conjugation to the porphyrin caused a change in the interaction between the AMP and the cell. These types of changes in binding behavior have been reported previously upon conjugation to surfaces.[4] Alternatively, the structural changes in the AMP occurring upon interaction of the indicator with the bacterial targets may be insufficient to cause changes in the spectrophotometric characteristics of the porphyrins. This could result from orientation of the porphyrin to the peptide or, more likely, the increased distance between the peptide "recognition" domain and the porphyrin "reporting" domain. Conversion of the C_1S_3TPP into an amine derivative and subsequent addition of the AMAS linker resulted in a ~10 Å tether between the porphyrin and the porphyrin moiety; this distance may exceed that necessary for effective transduction of a peptide conformational change into a localized environment change for the porphyrin.

Fig. 8 – C14-AMAS-Indol construct. Absorbance (A) and fluorescence (C) difference spectra for the interaction of C_1S_3TPP-Indol (indicator 16 μM) with *E. coli* (red; 1.9×10^6 cell/mL) and *B. cereus* (blue; 2.0×10^6 cell/mL). The concentration dependence of these changes is presented in Panels B and D. The green lines are the fits from Figure 7 (EDC/NHS construct). Complete data sets provided in Appendix B.

In order to further explore possible interactions between the C14-AMAS-Indol construct and the bacterial targets, the construct was added to microcentrifuge tubes with bacteria. Fluorescence was evaluated for this initial solution as well as for the pellet and supernatant following centrifugation of the tube. Analysis was completed based on the ratio of the concentration in the pellet to that of the original solution as calculated based on peak fluorescence (Figure 9). In a tube with no bacterial target, indicator concentrations in pellets containing EDC/NHS C_1S_3TPP-Indol construct were slightly higher than those of the initial solution (ratio = 1.06). The concentration of this indicator in the pellet increased (less indicator in the supernatant) as bacterial concentration increased (Figure 9). Increases in concentration were slightly more pronounced for *E. coli*. For the C14-AMAS-Indol indicator, increased concentrations in the pellets were noted for only the highest cell concentrations and were minimal for even those conditions (ratio = 1.4 versus 1.0 in absence of cells). This minimal accumulation tends to indicate that conjugation has caused a disruption of typical cell-peptide interaction behaviors.
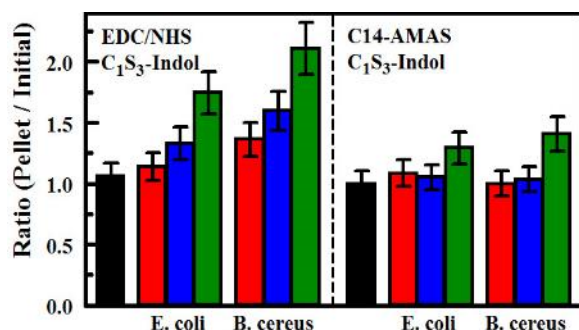
Fig. 9 - C14-AMAS-Indol pellet analysis. Ratio of peak fluorescence in the pellet following centrifuge to that of the initial target solution. For the two indicators, the black bar indicates results in the absence of bacterial cells. The remaining bars are for initial bacteria concentrations (left to right) for *E. coli* at 1.9×10^4, 1.9 x 10^5, and 1.9×10^6 cell/mL and for *B. cereus* at 2.0×10^4, 2.0 x 10^5, and 2.0×10^6 cell/mL. Initial concentration is 8 µM for the constructs.

The interaction of the C14-GMBS-Indol construct with *E. coli* and *B. cereus* produced only slight changes in the absorbance spectrum for even the highest concentrations of cells and indicators (Figure 10). Changes in fluorescence emission were more pronounced, with differing sensitivity between the two targets. Though the changes in absorbance appear to be different for the two types of targets, these changes are of low intensity, making discrimination difficult. As noted above, the minimal changes in absorbance and fluorescence could indicate issues related to conjugation with the porphyrin or insufficiency in coupling of AMP structural changes to the porphyrin environment. Additional analysis following the pellet accumulation procedure showed some increases in concentration of indicator for the 10^5 and 10^6 cell concentrations (Figure 11). These were, however, significantly less than the increases observed for the EDC/NHS C_1S_3TPP-Indol construct. This minimal accumulation tends to indicate that conjugation has caused a disruption of typical cell-peptide interaction behaviors.
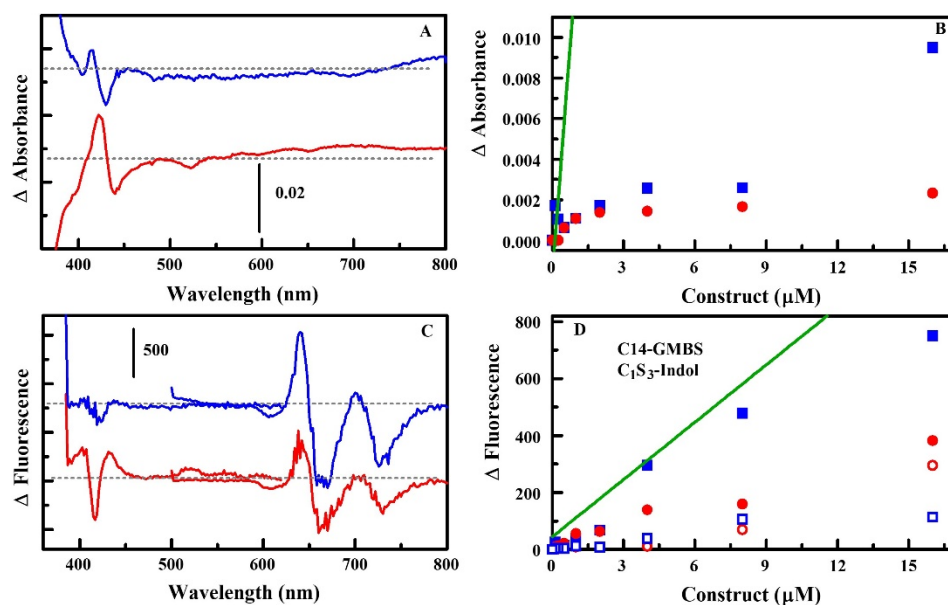

Fig. 10 – C14-GMBS-Indol construct. Absorbance (A) and fluorescence (C) difference spectra for the interaction of C_1S_3TPP-Indol (indicator 16 µM) with *E. coli* (red; 1.9×10^6 cell/mL) and *B. cereus* (blue; 2.0×10^6 cell/mL). The concentration dependence of these changes is presented in Panels B and D. The green lines are the fits from Figure 7 (EDC/NHS construct). Complete data sets provided in Appendix B.

Fig. 11 - C14-GMBS-Indol pellet analysis. Ratio of peak fluorescence in the pellet following centrifuge to that of the initial target solution. For the two indicators, the black bar indicates results in the absence of bacterial cells. The remaining bars are for initial bacteria concentrations (left to right) for *E. coli* at 1.9×10^4, 1.9×10^5, and 1.9×10^6 cell/mL and for *B. cereus* at 2.0×10^4, 2.0×10^5, and 2.0×10^6 cell/mL. Initial concentration is 8 μM for the constructs.
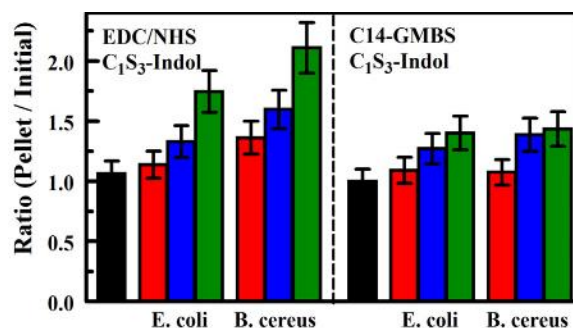
The interaction of the C14-EMCS-Indol construct with *E. coli* and *B. cereus* produced only small changes in absorbance for even the highest concentrations of cells and indicators (Figure 12). Changes in fluorescence were slightly more pronounced. As noted above, the minimal changes in absorbance could indicate issues related to conjugation with the porphyrin or insufficiency in coupling of AMP structural changes to the porphyrin environment. Additional analysis following the pellet accumulation procedure showed increases in concentration of indicator in the pellet for the 10^6 cell concentrations; changes were significant in the case of *E. coli* (Figure 13). Increases for *B. cereus* were less than those observed for the EDC/NHS C_1S_3TPP-Indol construct. Given the minimal accumulation of peptide in the presence of *B. cereus*, it seems likely that conjugation to the porphyrin caused some changes in the interaction between the AMP and bacterial cells.

Fig. 12 – C14-EMCS-Indol construct. Absorbance (A) and fluorescence (C) difference spectra for the interaction of C_1S_3TPP-Indol (indicator 16 μM) with *E. coli* (red; 1.9×10^6 cell/mL) and *B. cereus* (blue; 2.0×10^6 cell/mL). The concentration dependence of these changes is presented in Panels B and D. The green lines are the fits from Figure 7 (EDC/NHS construct). Complete data sets provided in Appendix B.
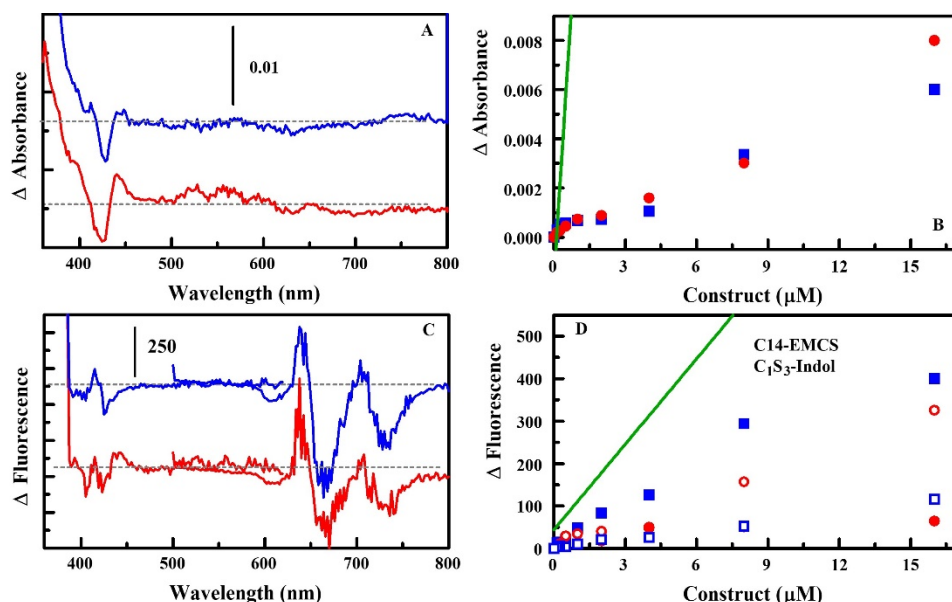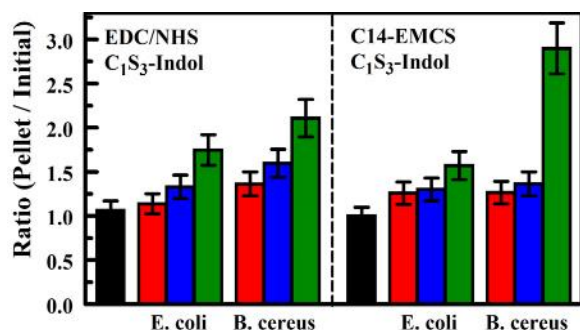
Fig. 13 - C14-EMCS-Indol pellet analysis. Ratio of peak fluorescence in the pellet following centrifuge to that of the initial target solution. For the two indicators, the black bar indicates results in the absence of bacterial cells. The remaining bars are for initial bacteria concentrations (left to right) for *E. coli* at 1.9×10^4, 1.9×10^5, and 1.9×10^6 cell/mL and for *B. cereus* at 2.0×10^4, 2.0×10^5, and 2.0×10^6 cell/mL. Initial concentration is 8 µM for the constructs.

The interaction of the C14-MBS-Indol construct with *E. coli* and *B. cereus* produced only slight changes in the absorbance spectrum for even the highest concentrations of cells and indicators (Figure 14). Changes in fluorescence emission were more pronounced, primarily upon interaction with *B. cereus*. All changes in intensity were less than those observed for the EDC/NHS construct. Though changes in absorbance appear to be different for the two types of targets, these changes are of low intensity, making discrimination difficult. As noted above, the minimal changes in absorbance and fluorescence could indicate issues related to conjugation with the porphyrin or insufficiency in coupling of AMP structural changes to the porphyrin environment. Additional analysis following the pellet accumulation procedure showed some concentration dependent accumulation of indicator in the pellet (Figure 15). This behavior was, however, significantly less pronounced than the increases observed for the EDC/NHS C_1S_3TPP-Indol construct. This minimal accumulation tends to indicate that conjugation has caused a disruption of typical cell-peptide interaction behaviors.
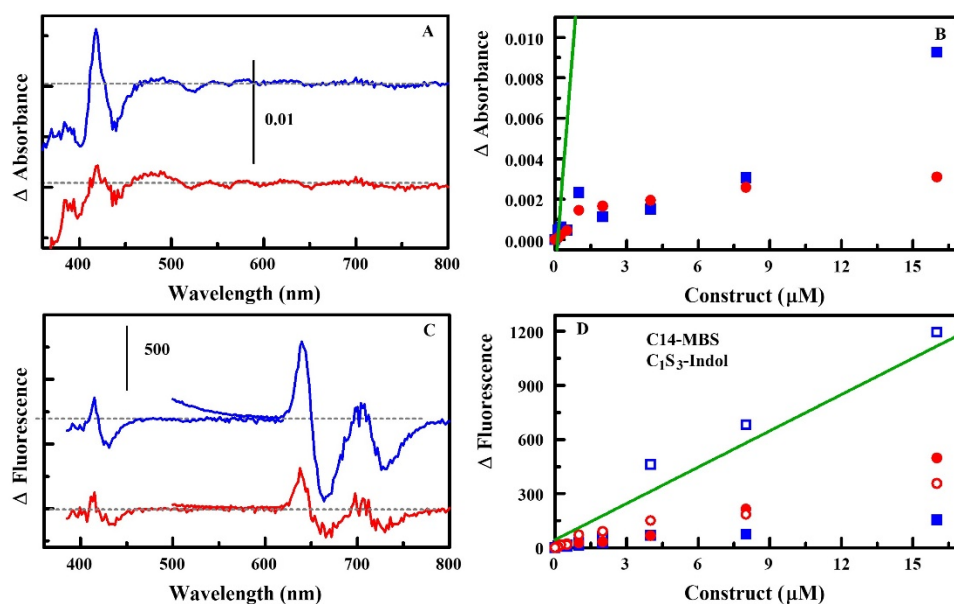

Fig. 14 – C14-MBS-Indol construct. Absorbance (A) and fluorescence (C) difference spectra for the interaction of C_1S_3TPP-Indol (indicator 16 µM) with *E. coli* (red; 1.9×10^6 cell/mL) and *B. cereus* (blue; 2.0×10^6 cell/mL). The concentration dependence of these changes is presented in Panels B and D. The green lines are the fits from Figure 7 (EDC/NHS construct). Complete data sets provided in Appendix B.

Fig. 15 - C14-MBS-Indol pellet analysis. Ratio of peak fluorescence in the pellet following centrifuge to that of the initial target solution. For the two indicators, the black bar indicates results in the absence of bacterial cells. The remaining bars are for initial bacteria concentrations (left to right) for *E. coli* at 1.9×10^4, 1.9×10^5, and 1.9×10^6 cell/mL and for *B. cereus* at 2.0×10^4, 2.0×10^5, and 2.0×10^6 cell/mL. Initial concentration is 8 µM for the constructs.
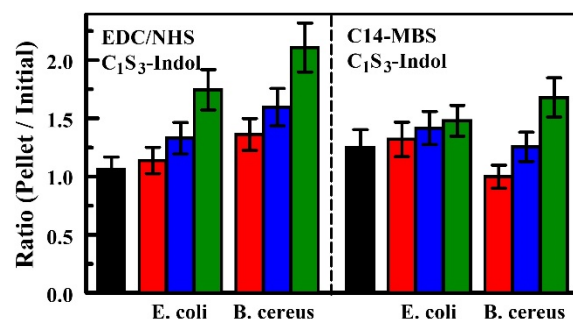
The interaction of the C14-SMCC-Indol construct with *E. coli* and *B. cereus* produced only slight changes in the absorbance spectrum for even the highest concentrations of cells and indicators (Figure 16). Changes in fluorescence emission were slightly more pronounced with similar sensitivity to the two targets. All changes in intensity were less than those observed for the EDC/NHS construct. As noted above, the minimal changes in absorbance and fluorescence could indicate issues related to conjugation with the porphyrin or insufficiency in coupling of AMP structural changes to the porphyrin environment. Additional analysis following the pellet accumulation procedure showed concentration dependent accumulation of indicator in the pellet primarily at the 10^6 concentrations (Figure 17). The analysis indicates interaction of the C14-SMCC-Indol indicator with both bacterial targets, but affinity may have been impacted by the conjugation process.
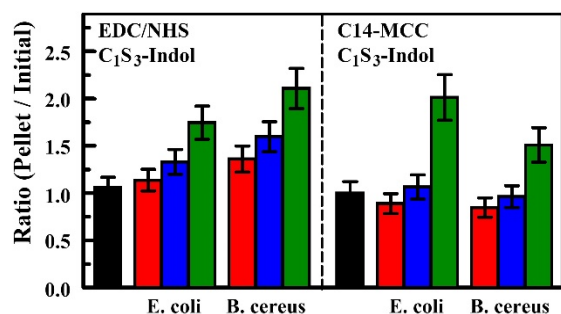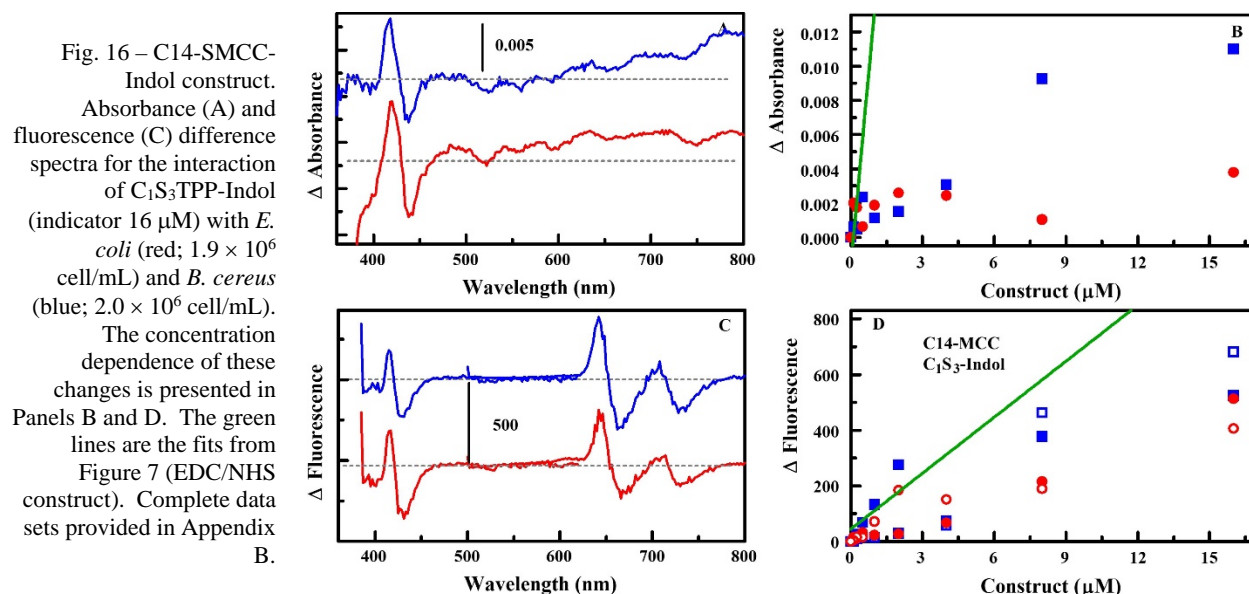
Fig. 16 – C14-SMCC-Indol construct. Absorbance (A) and fluorescence (C) difference spectra for the interaction of C_1S_3TPP-Indol (indicator 16 µM) with *E. coli* (red; 1.9×10^6 cell/mL) and *B. cereus* (blue; 2.0×10^6 cell/mL). The concentration dependence of these changes is presented in Panels B and D. The green lines are the fits from Figure 7 (EDC/NHS construct). Complete data sets provided in Appendix B.

Fig. 17 - C14-SMCC-Indol pellet analysis. Ratio of peak fluorescence in the pellet following centrifuge to that of the initial target solution. For the two indicators, the black bar indicates results in the absence of bacterial cells. The remaining bars are for initial bacteria concentrations (left to right) for *E. coli* at 1.9×10^4, 1.9×10^5, and 1.9×10^6 cell/mL and for *B. cereus* at 2.0×10^4, 2.0×10^5, and 2.0×10^6 cell/mL. Initial concentration is 8 µM for the constructs.

C1-Indol constructs.

The interaction of the C1-AMAS-Indol construct with *E. coli* and *B. cereus* produced only slight changes in the absorbance spectrum for even the highest concentrations of cells and indicators. As shown in Figure 18, changes in the spectrophotometric characteristics of this construct are significantly smaller than those noted for the EDC/NHS construct. The minimal changes in absorbance and fluorescence could indicate that conjugation to the porphyrin caused a change in the interaction between the AMP and the cell. These types of changes in binding behavior have been reported previously upon conjugation to surfaces.[4] Alternatively, the structural changes in the AMP occurring upon interaction of the indicator with the bacterial targets may be insufficient to cause changes in the spectrophotometric characteristics of the porphyrins. This could result from orientation of the porphyrin to the peptide or increased distance between the two. Additional analysis following the pellet accumulation procedure showed increases in pellet indicator concentrations in the presence of the bacterial cells (Figure 19). These changes were larger than the increases observed for the EDC/NHS C_1S_3TPP-Indol construct. This analysis tends to indicate significant interaction between the C1-AMAS-Indol indicator and both bacterial targets. Unfortunately, it is not clear that this interaction will produce the necessary changes in the spectrophotometric characteristics of the porphyrin for a sensing application.
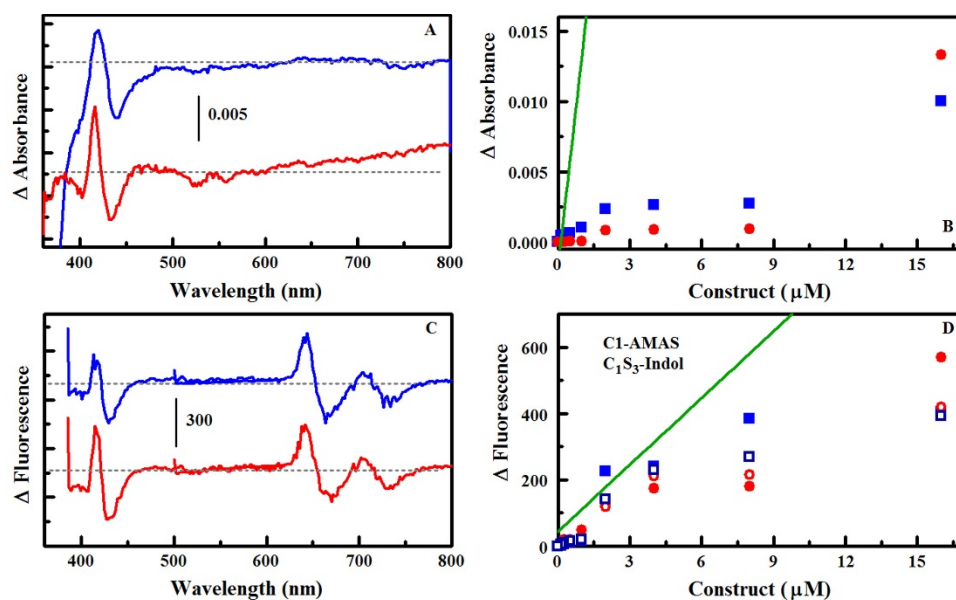

Fig. 18 – C1-AMAS-Indol construct. Absorbance (A) and fluorescence (C) difference spectra for the interaction of C_1S_3TPP-Indol (indicator 16 μM) with *E. coli* (red; 1.9×10^6 cell/mL) and *B. cereus* (blue; 2.0×10^6 cell/mL). The concentration dependence of these changes is presented in Panels B and D. The green lines are the fits from Figure 7 (EDC/NHS construct). Complete data sets provided in Appendix C.
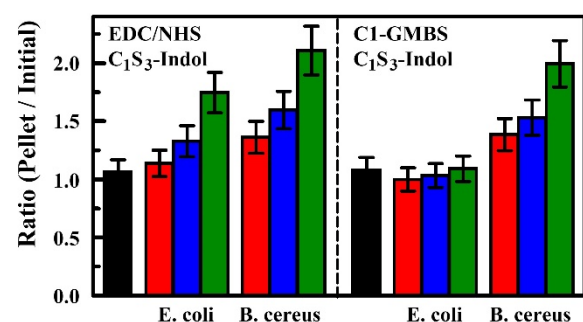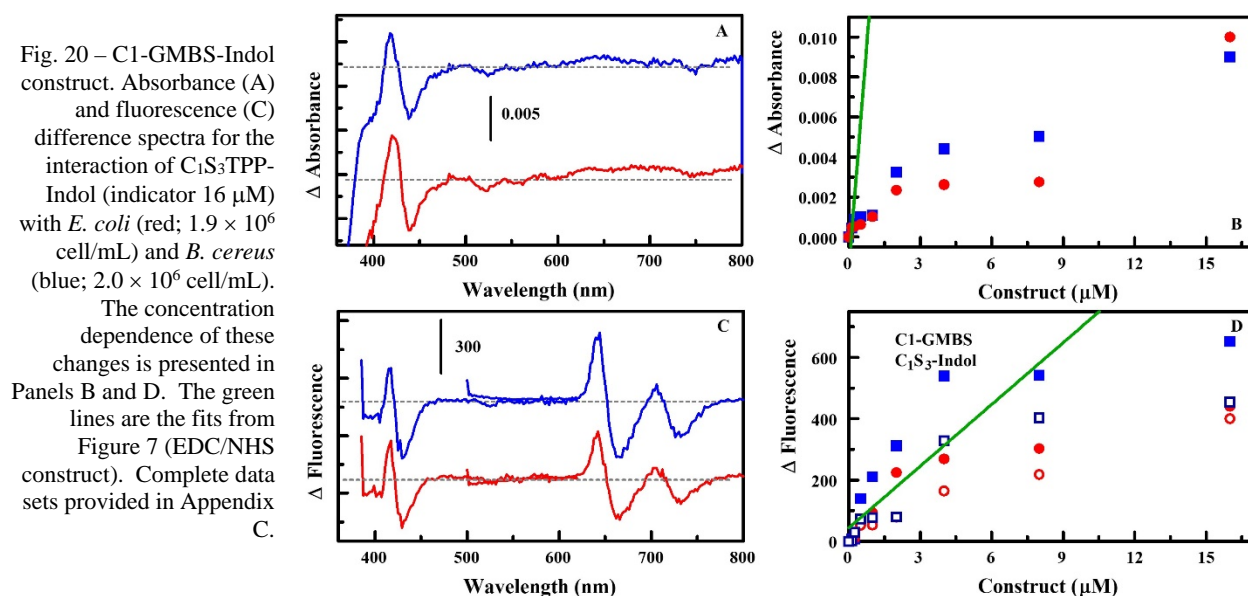

Fig. 19 - C1-AMAS-Indol pellet analysis. Ratio of peak fluorescence in the pellet following centrifuge to that of the initial target solution. For the two indicators, the black bar indicates results in the absence of bacterial cells. The remaining bars are for initial bacteria concentrations (left to right) for *E. coli* at 1.9×10^4, 1.9×10^5, and 1.9×10^6 cell/mL and for *B. cereus* at 2.0×10^4, 2.0×10^5, and 2.0×10^6 cell/mL. Initial concentration is 8 μM for the constructs.
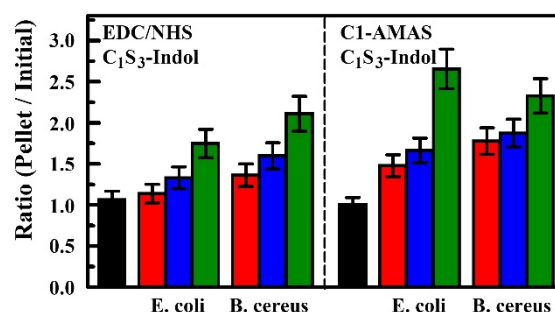
The interaction of the C1-GMBS-Indol construct with *E. coli* and *B. cereus* produced only slight changes in the absorbance spectrum for even the highest concentrations of cells and indicators. As shown in Figure 20, changes in the spectrophotometric characteristics of this construct are significantly smaller than those noted for the EDC/NHS construct. The changes in fluorescence, while still of lower intensity than those of the EDC/NHS construct, were more significant. As noted above, low intensity changes in absorbance and fluorescence could indicate issues related to conjugation with the porphyrin or insufficiency in coupling of AMP structural changes to the porphyrin environment. Additional analysis following the pellet accumulation procedure showed increases in concentration of indicator in the pellet for *E. coli* (Figure 21). Increases in concentration were not noted for *B. cereus*. This difference in accumulation behavior tends to indicate that conjugation has caused a disruption of typical cell-peptide interaction behaviors.
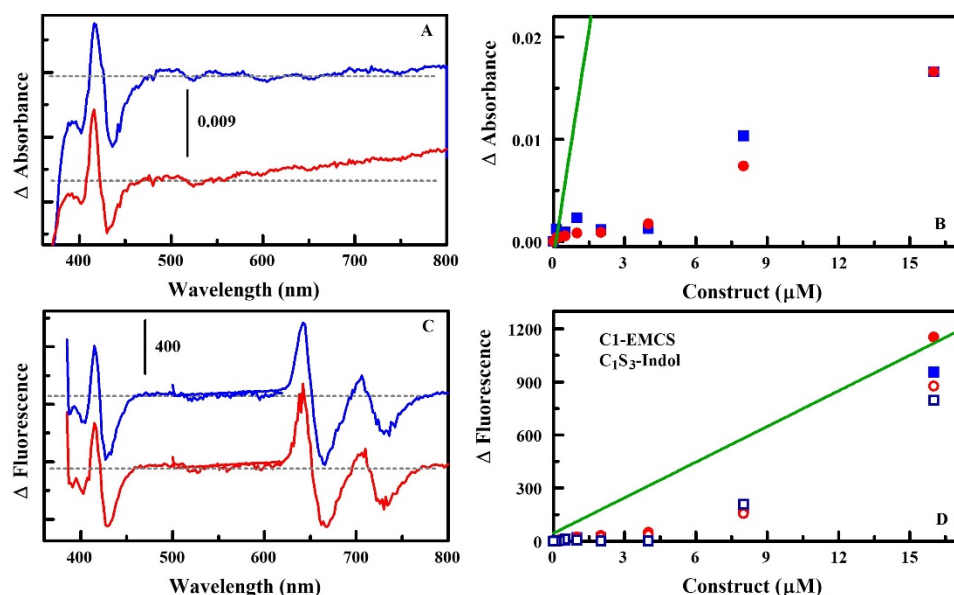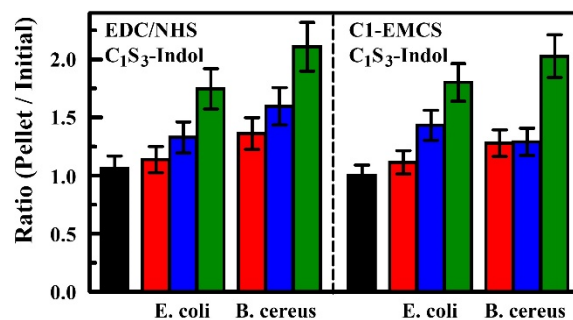

Fig. 20 – C1-GMBS-Indol construct. Absorbance (A) and fluorescence (C) difference spectra for the interaction of C_1S_3TPP-Indol (indicator 16 µM) with *E. coli* (red; 1.9×10^6 cell/mL) and *B. cereus* (blue; 2.0×10^6 cell/mL). The concentration dependence of these changes is presented in Panels B and D. The green lines are the fits from Figure 7 (EDC/NHS construct). Complete data sets provided in Appendix C.

Fig. 21 - C1-GMBS-Indol pellet analysis. Ratio of peak fluorescence in the pellet following centrifuge to that of the initial target solution. For the two indicators, the black bar indicates results in the absence of bacterial cells. The remaining bars are for initial bacteria concentrations (left to right) for *E. coli* at 1.9×10^4, 1.9×10^5, and 1.9×10^6 cell/mL and for *B. cereus* at 2.0×10^4, 2.0×10^5, and 2.0×10^6 cell/mL. Initial concentration is 8 µM for the constructs.

The interaction of the C1-EMCS-Indol construct with *E. coli* and *B. cereus* produced only moderate changes in the absorbance spectrum for even the highest concentrations of cells and indicators. As shown in Figure 22, changes in the spectrophotometric (absorbance and fluorescence) characteristics of this construct are noted only for the two highest concentrations considered. As noted above, the minimal changes in absorbance and fluorescence could indicate issues related to conjugation with the porphyrin or insufficiency in coupling of AMP conformational changes to the porphyrin environment. Additional analysis following the pellet accumulation procedure showed increases in concentration of indicator in the pellet for *E. coli* (Figure 23). Increases in concentration were noted for only the highest concentration of *B. cereus*. This analysis tends to indicate interaction between the C1-EMCS-Indol indicator and both bacterial targets. Unfortunately, it is not clear that this interaction will be of sufficient affinity or will produce the necessary changes in the spectrophotometric characteristics of the porphyrin for use in a sensing application.
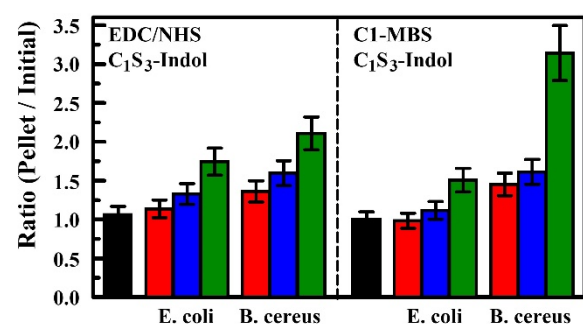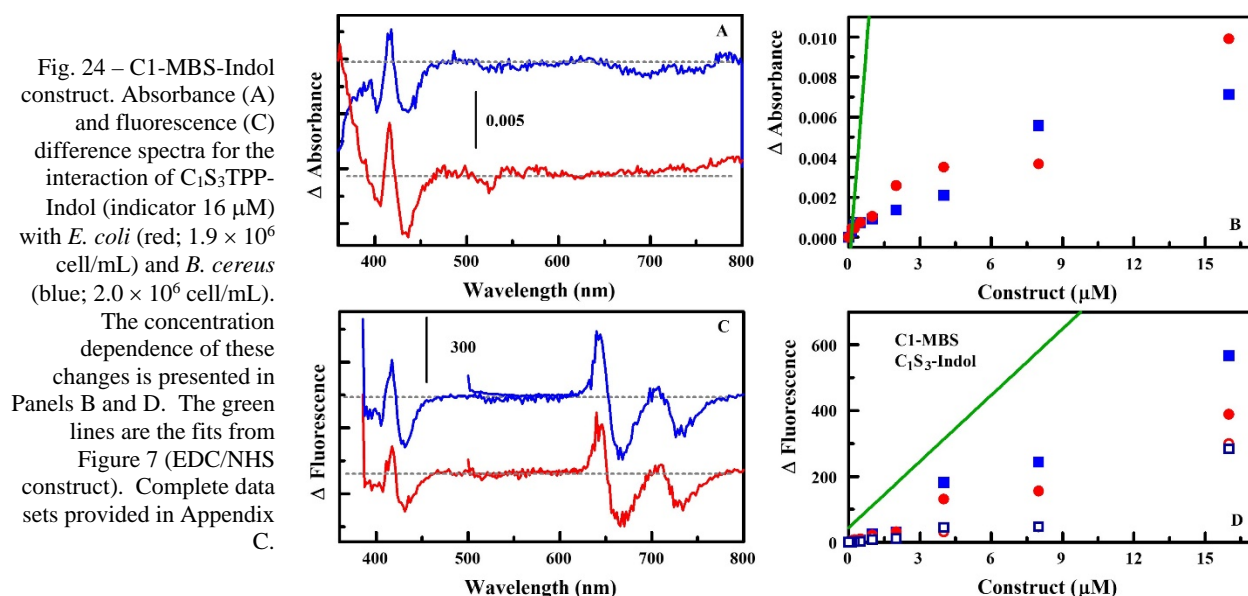

Fig. 22 – C1-EMCS-Indol construct. Absorbance (A) and fluorescence (C) difference spectra for the interaction of C_1S_3TPP-Indol (indicator 16 μM) with *E. coli* (red; 1.9×10^6 cell/mL) and *B. cereus* (blue; 2.0×10^6 cell/mL). The concentration dependence of these changes is presented in Panels B and D. The green lines are the fits from Figure 7 (EDC/NHS cosntruct). Complete data sets provided in Appendix C.

Fig. 23 - C1-EMCS-Indol pellet analysis. Ratio of peak fluorescence in the pellet following centrifuge to that of the initial target solution. For the two indicators, the black bar indicates results in the absence of bacterial cells. The remaining bars are for initial bacteria concentrations (left to right) for *E. coli* at 1.9×10^4, 1.9×10^5, and 1.9×10^6 cell/mL and for *B. cereus* at 2.0×10^4, 2.0×10^5, and 2.0×10^6 cell/mL. Initial concentration is 8 μM for the constructs.

   The interaction of the C1-MBS-Indol construct with *E. coli* and *B. cereus* produced only slight changes in the absorbance and fluorescence spectra for even the highest concentrations of cells and indicators. As shown in Figure 24, although dose-responsive, changes in the spectrophotometric characteristics of this construct are significantly smaller than those noted for the EDC/NHS construct. As noted above, the minimal changes in absorbance and fluorescence could indicate issues related to conjugation with the porphyrin or insufficiency in coupling of AMP conformational changes to the porphyrin environment. Additional analysis following the pellet accumulation procedure showed some increases in pellet indicator concentrations for *B. cereus* (Figure 24). Changes in concentration for *E. coli* were less significant. This analysis tends to indicate interaction between the C1-MBS-Indol indicator and both bacterial targets. Unfortunately, it is not clear that this interaction will be of sufficient affinity or will produce the necessary changes in the spectrophotometric characteristics of the porphyrin for use in a sensing application.
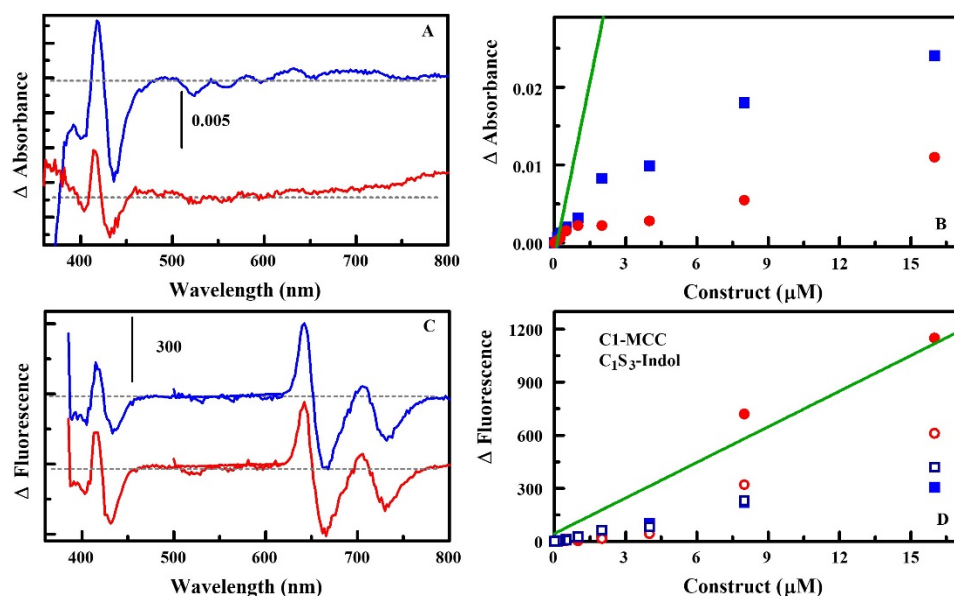

Fig. 24 – C1-MBS-Indol construct. Absorbance (A) and fluorescence (C) difference spectra for the interaction of C_1S_3TPP-Indol (indicator 16 μM) with *E. coli* (red; 1.9×10^6 cell/mL) and *B. cereus* (blue; 2.0×10^6 cell/mL). The concentration dependence of these changes is presented in Panels B and D. The green lines are the fits from Figure 7 (EDC/NHS construct). Complete data sets provided in Appendix C.

Fig. 25 - C1-MBS-Indol pellet analysis. Ratio of peak fluorescence in the pellet following centrifuge to that of the initial target solution. For the two indicators, the black bar indicates results in the absence of bacterial cells. The remaining bars are for initial bacteria concentrations (left to right) for *E. coli* at 1.9×10^4, 1.9×10^5, and 1.9×10^6 cell/mL and for *B. cereus* at 2.0×10^4, 2.0×10^5, and 2.0×10^6 cell/mL. Initial concentration is 8 μM for the constructs.

The interaction of the C1-SMCC-Indol construct with *E. coli* and *B. cereus* produced moderate changes in the absorbance spectrum as well as changes in fluorescence. As shown in Figure 26, absorbance changes were less significant than those noted for the EDC/NHS construct, although fluorescence changes are on a similar scale as those for the EDC/NHS construct. As noted above, changes in spectrophotometric characteristics are dependent on conjugation to the porphyrin with sufficient coupling of AMP structural changes to the porphyrin environment. Additional analysis following the pellet accumulation procedure showed concentration dependent accumulation of the indicator in the pellet. Increases were similar to those observed for the EDC/NHS C_1S_3TPP-Indol construct (Figure 27). This analysis tends to indicate interaction between the C1-SMCC-Indol indicator and both bacterial targets. Additional analysis in the paper supported format will be necessary to determine if the affinity and binding induced changes in the spectrophotometric characteristics of the porphyrin are sufficient for use in the sensing application.

Fig. 26 – C1-SMCC-Indol construct. Absorbance (A) and fluorescence (C) difference spectra for the interaction of C_1S_3TPP-Indol (indicator 16 μM) with *E. coli* (red; 1.9×10^6 cell/mL) and *B. cereus* (blue; 2.0×10^6 cell/mL). The concentration dependence of these changes is presented in Panels B and D. The green lines are the fits from Figure 7 (EDC/NHS construct). Complete data sets provided in Appendix C.

Fig. 27 - C1-SMCC-Indol pellet analysis. Ratio of peak fluorescence in the pellet following centrifuge to that of the initial target solution. For the two indicators, the black bar indicates results in the absence of bacterial cells. The remaining bars are for initial bacteria concentrations (left to right) for *E. coli* at 1.9×10^4, 1.9×10^5, and 1.9×10^6 cell/mL and for *B. cereus* at 2.0×10^4, 2.0×10^5, and 2.0×10^6 cell/mL. Initial concentration is 8 μM for the constructs.
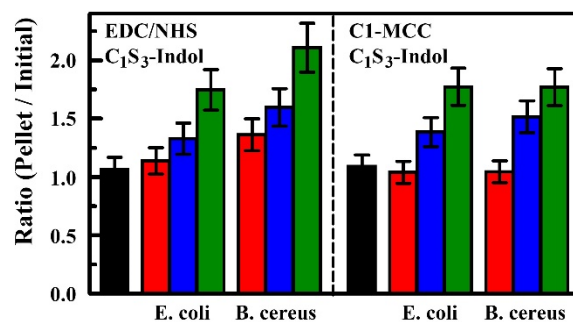
CONCLUSIONS

We have demonstrated the potential of porphyrin modified AMPs for indication of bacterial targets on the basis of changes in the spectrophotometric characteristics of the construct.[9 ,10] The approach can be applied only with peptides providing a change in conformation upon target interaction. Here, we investigated additional methods for conjugation of the porphyrin indicator to the AMP indolicidin. The intention was to provide functional constructs that could be assembled with more control over the point of

modification and the ratio of porphyrin to peptide. The analysis presented here indicates that C1 modifications are more likely to offer the types of functional constructs necessary to our application. Unfortunately, none of the crosslinked constructs offered changes in absorbance characteristics that were as large as those observed for the EDC/NHS construct. Some of the crosslinked constructs fail to interact with the bacterial targets in a substantial way, indicating that conjugation has impaired the typical peptide/cell interactions. In other cases, the peptide constructs interact with the targets, but the changes in the spectrophotometric characteristics of the porphyrin are minimal. The C1-SMCC, C1-MBS, C1-AMAS, and C1-EMCS constructs interact with both bacterial targets and show slight to moderate changes in spectrophotometric characteristics upon target interaction. Analysis of these materials in the paper supported format utilized for the intended sensing approach will be necessary to assess final utility.

The porphyrin-peptide constructs evaluated here are intended to enable a new type of biosensing approach. Because the construct offers both target recognition and optical transduction, no additional reagents are necessary (e.g., labeled antibody or non-specific dye). The constructs in this study were utilized in solution, but we are currently working with paper supported porphyrin-peptide constructs. An immobilized array will enable use of these constructs with either fluorescence-based [11] or reflectance-based detectors. [12] As in previously described work, the response of an array of indicators can be utilized to classify the targets detected, [1, 13] where a single indicator would not provide sufficient information for identification or classification.

ACKNOWLEDGEMENTS

REFERENCES

1. N.V. Kulagina; G.P. Anderson; F.S. Ligler; K.M. Shaffer; C.R. Taitt, "Antimicrobial peptides: New recognition molecules for detecting botulinum toxins," *Sensors* **7**, 2808-2824 (2007).
2. N.V. Kulagina; K.M. Shaffer; G.P. Anderson; F.S. Ligler; C.R. Taitt, "Antimicrobial peptide-based array for *Escherichia coli* and *Salmonella* screening," *Analytica Chimica Acta* **575**, 9-15 (2006).
3. M.M. Ngundi; N.V. Kulagina; G.P. Anderson; C.R. Taitt, "Nonantibody-based recognition: alternative molecules for detection of pathogens," *Expert Review of Proteomics* **3**, 511-524 (2006).
4. S.H. North; J. Wojciechowski; V. Chu; C.R. Taitt, "Surface immobilization chemistry influences peptide-based detection of lipopolysaccharide and lipoteichoic acid," *Journal of Peptide Science* **18**, 366-372 (2012).
5. C.R. Taitt; L.C. Shriver-Lake; M.M. Ngundi; F.S. Ligler, "Array Biosensor for Toxin Detection: Continued Advances," *Sensors* **8**, 8361-8377 (2008).
6. L. Baldini; A.J. Wilson; J. Hong; A.D. Hamilton, "Pattern-based detection of different proteins using an array of fluorescent protein surface receptors," *Journal of the American Chemical Society* **126**, 5656-5657 (2004).
7. L.K. Tsou; R.K. Jain; A.D. Hamilton, "Protein surface recognition by porphyrin-based receptors," *Journal of Porphyrins and Phthalocyanines* **8**, 141-147 (2004).

8. H.C. Zhou; L. Baldini; J. Hong; A.J. Wilson; A.D. Hamilton, "Pattern recognition of proteins based on an array of functionalized porphyrins," *Journal of the American Chemical Society* **128**, 2421-2425 (2006).

9. B.J. Johnson; C.R. Taitt; A. Gleaves; S.H. North; A.P. Malanoski; I.A. Leska; E. Archibong; S.M. Monk, "Porphyrin-modified antimicrobial peptide indicators for detection of bacteria," *Sensing and Bio-Sensing Research* **8**, 1-7 (2016).

10. B.J. White; C.R. Taitt; A. Gleaves; E. Archibong; S.M. Monk; I.A. Leska *Colorimetric Biosensor: Porphyrin Variations*; Naval Research Laboratory: 2018.

11. C.A. Rowe-Taitt; J.P. Golden; M.J. Feldstein; J.J. Cras; K.E. Hoffman; F.S. Ligler, "Array biosensor for detection of biohazards," *Biosensors & Bioelectronics* **14**, 785-794 (2000).

12. B. Johnson-White; J. Golden, "Reduction of background signal in automated array biosensors," *Measurement Science & Technology* **16**, N29-N31 (2005).

13. C.R. Taitt; S.H. North; N.V. Kulagina, "Antimicrobial peptide arrays for detection of inactivated biothreat agents," *Methods in Molecular Biology* **570**, 233-255 (2009).

APPENDIX A

EDC/NHS C$_1$S$_3$TPP-INDOL

Figure A1. The EDC/NHS C_1S_3-Indol indicator. Absorbance (left) and fluorescence (right) spectra for the C_1S_3-Indol construct (concentrations in μM provided in the legend). Below, the peak intensity versus concentration is provided. All compounds in 15% DMSO.
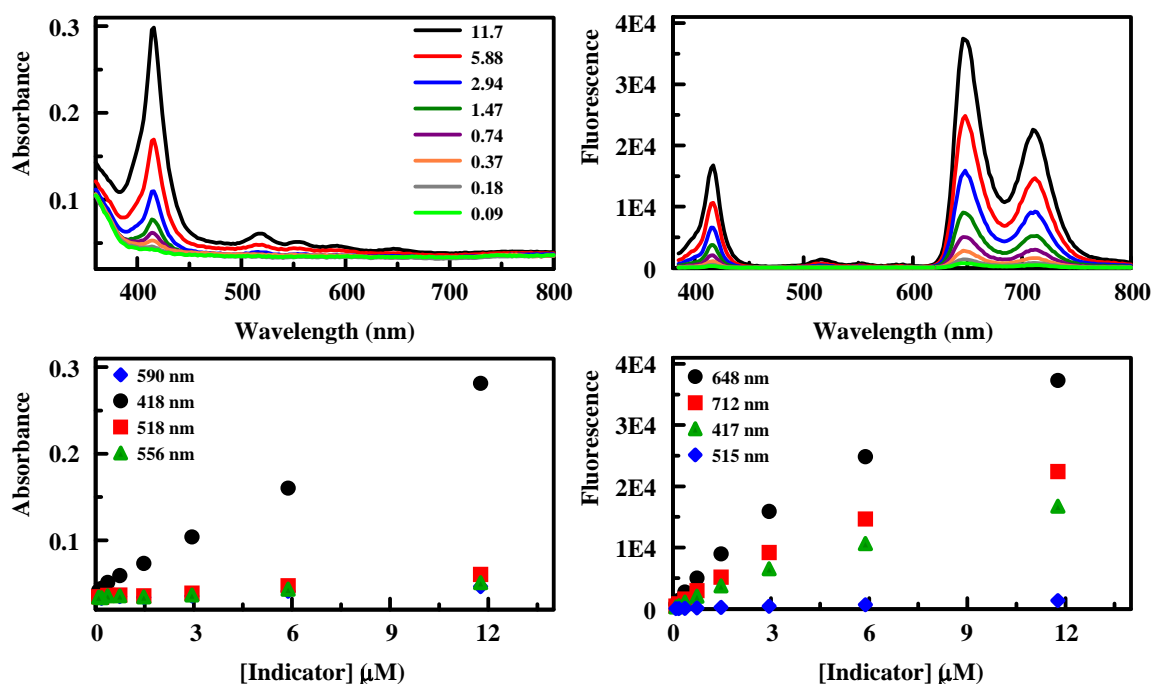
Figure A2. Interaction of EDC/NHS C_1S_3-Indol with *E. coli*. Absorbance (left) and fluorescence (right) spectra for C_1S_3-Indol (11.8 μM) in the presence and absence (black) of bacterial cells (concentrations in cells/mL provided in the legend). All solutions contain 15% DMSO.
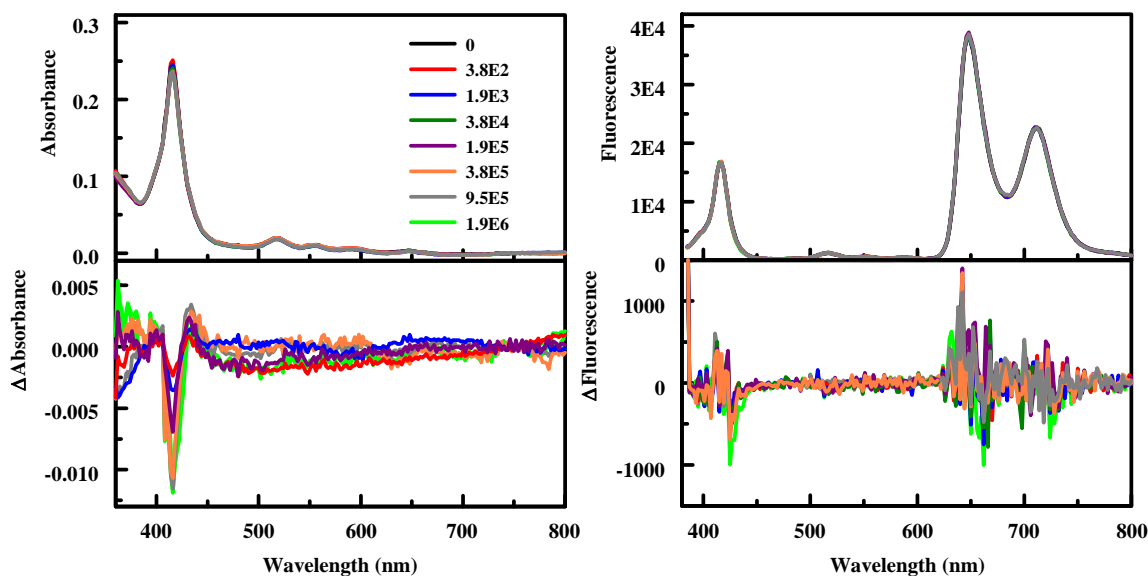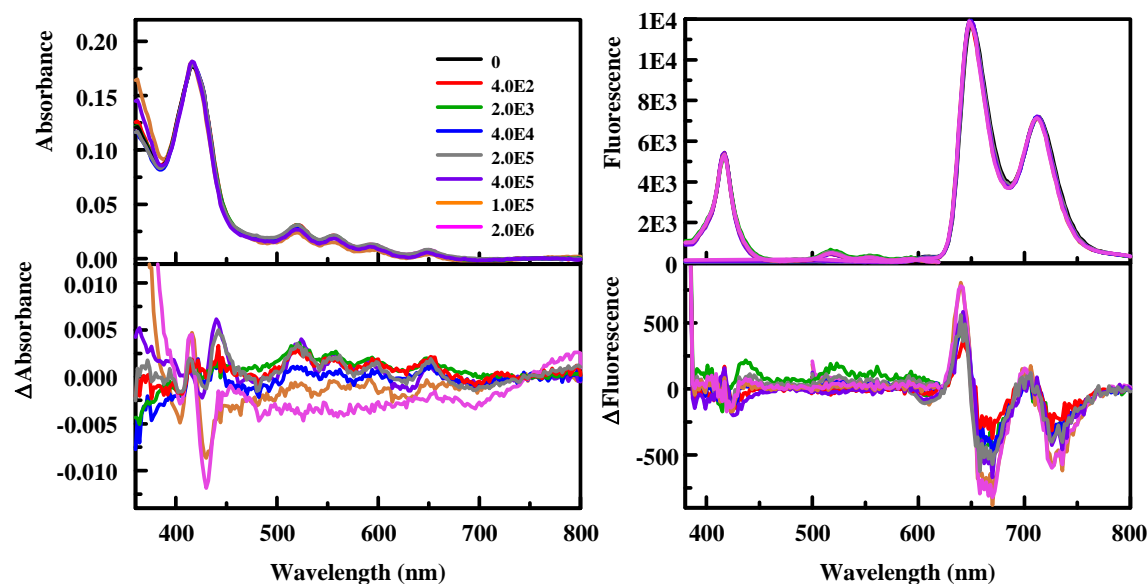
Figure A3. Interaction of EDC/NHS C_1S_3-Indol with *B. cereus*. Absorbance (left) and fluorescence (right) spectra for C_1S_3-Indol (11.8 μM) in the presence and absence (black) of bacterial cells (concentrations in cells/mL provided in the legend). All solutions contain 15% DMSO.
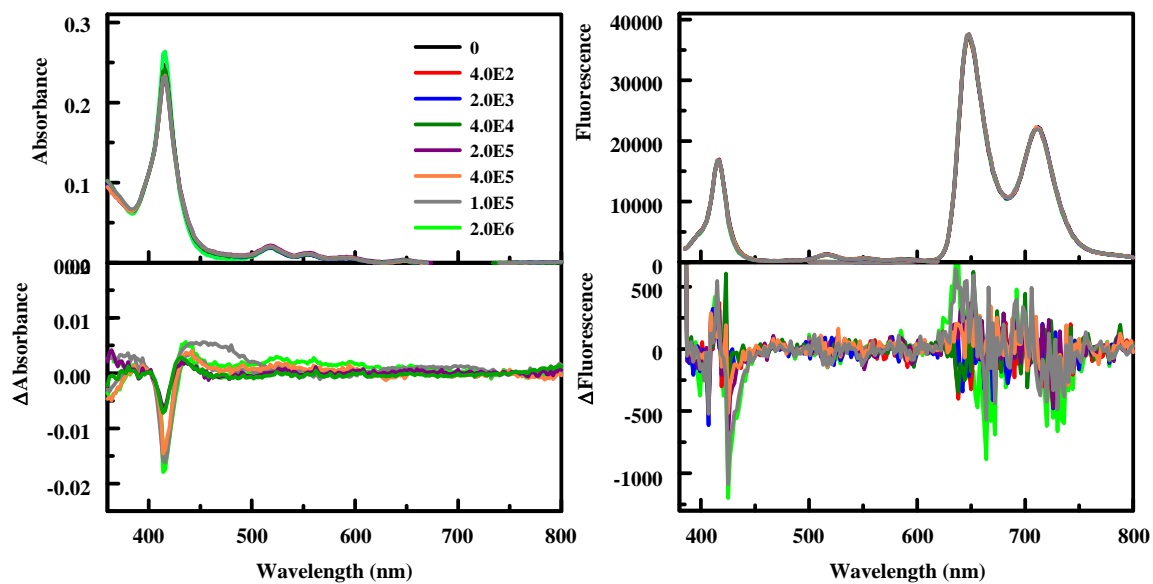
APPENDIX B

C14-INDOL CROSSLINKED C$_1$S$_3$TPP CONSTRUCTS

Figure B1. C14-AMAS-Indol. Absorbance (left) and fluorescence (right) characteristics for the AMAS crosslinked C_1S_3TPP modified C14-Indol. All spectra were collected in 15% DMSO. Tracer concentrations are provided in the legend (µM).
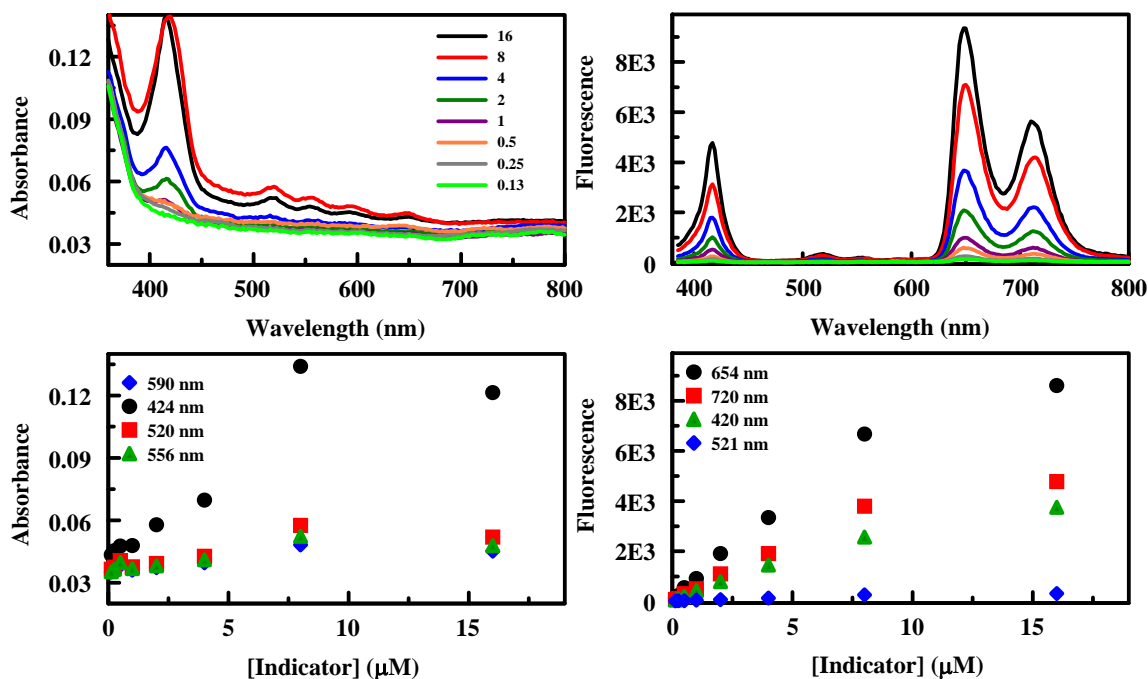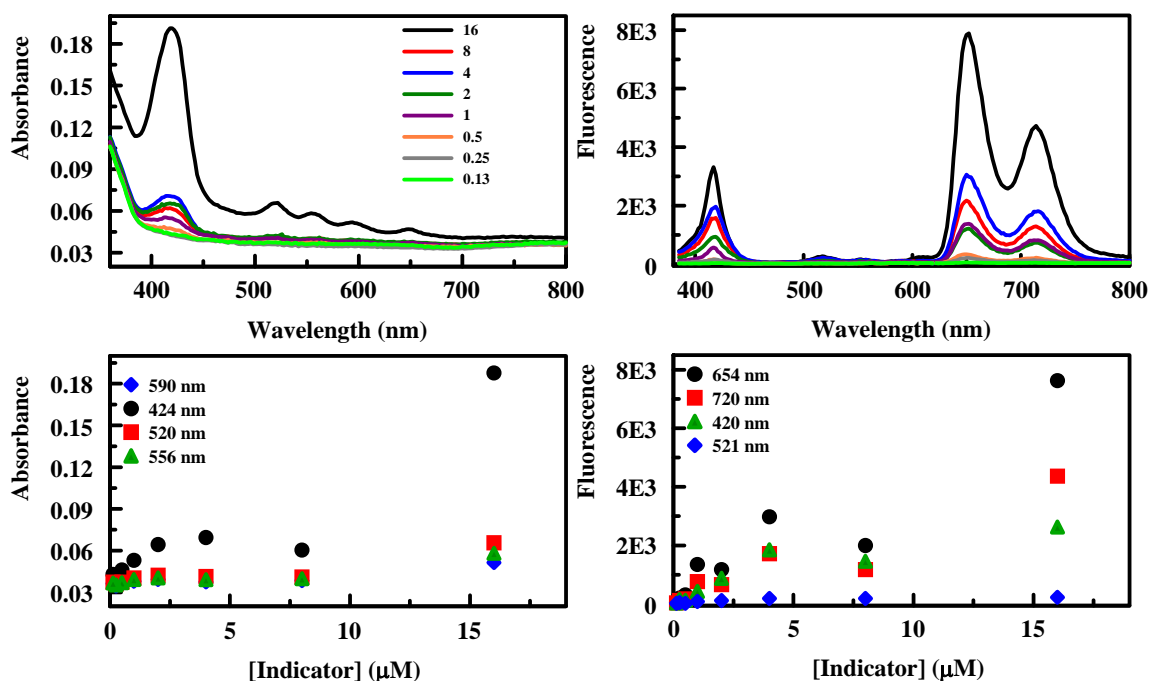

Figure B2. Interaction of C14-AMAS-Indol with *E. coli*. Absorbance (left) and fluorescence (right) spectra for C_1S_3-Indol (16 µM) in the presence and absence (black) of bacterial cells (concentrations in cells/mL provided in the legend). All solutions contain 15% DMSO.
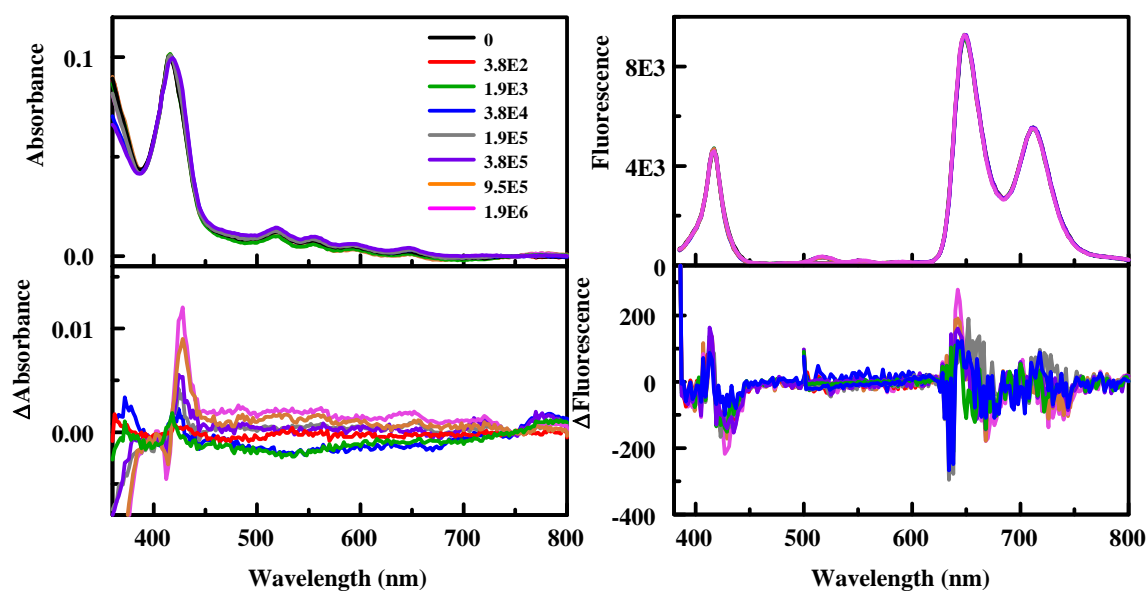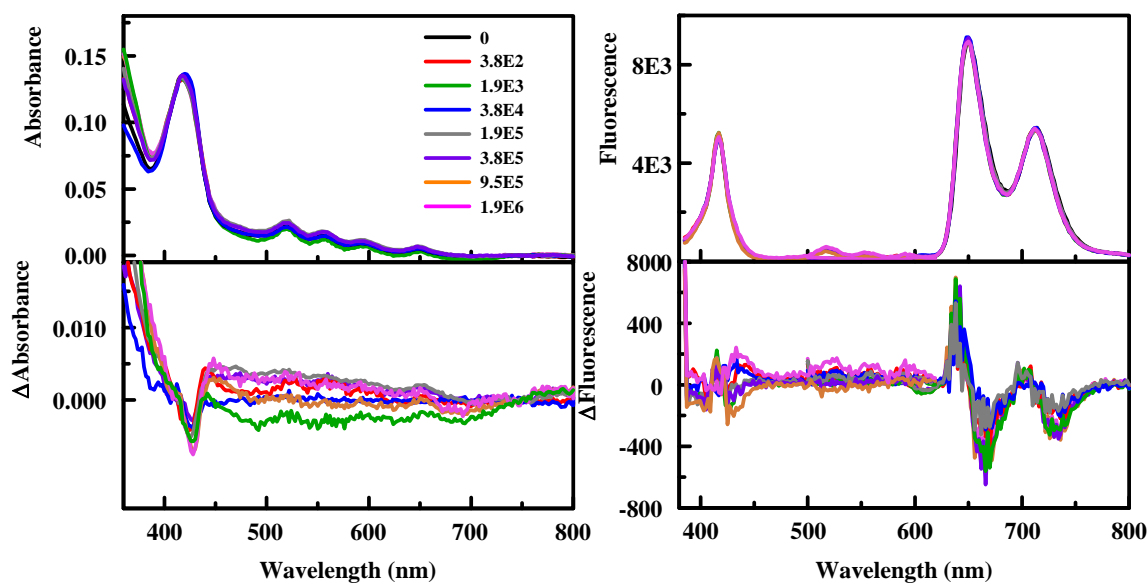
Figure B3. Interaction of C14-AMAS-Indol with *B. cereus*. Absorbance (left) and fluorescence (right) spectra for C_1S_3-Indol (16 μM) in the presence and absence (black) of bacterial cells (concentrations in cells/mL provided in the legend). All solutions contain 15% DMSO.
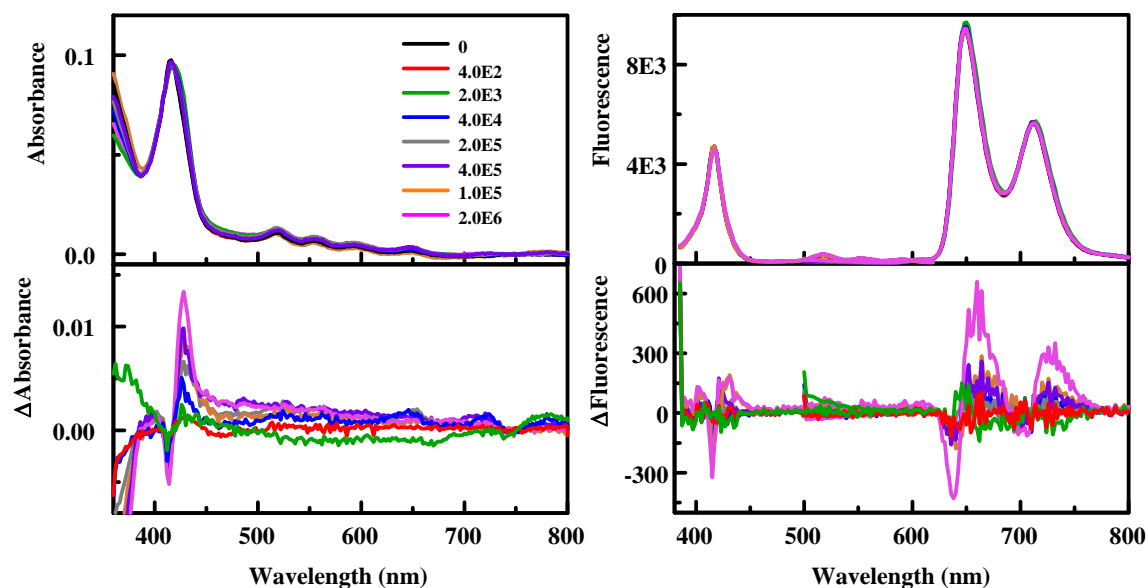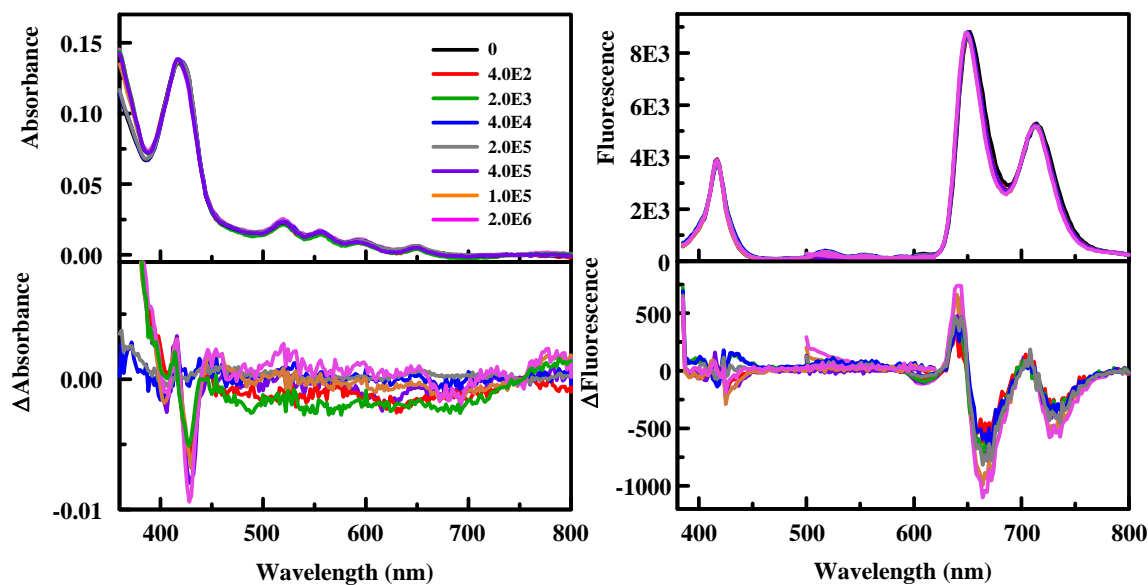

Figure B4. C14-GMBS-Indol. Absorbance (left) and fluorescence (right) characteristics for the EMBS crosslinked C_1S_3TPP modified C14-Indol. All spectra were collected in 15% DMSO. Tracer concentrations are provided in the legend (μM).
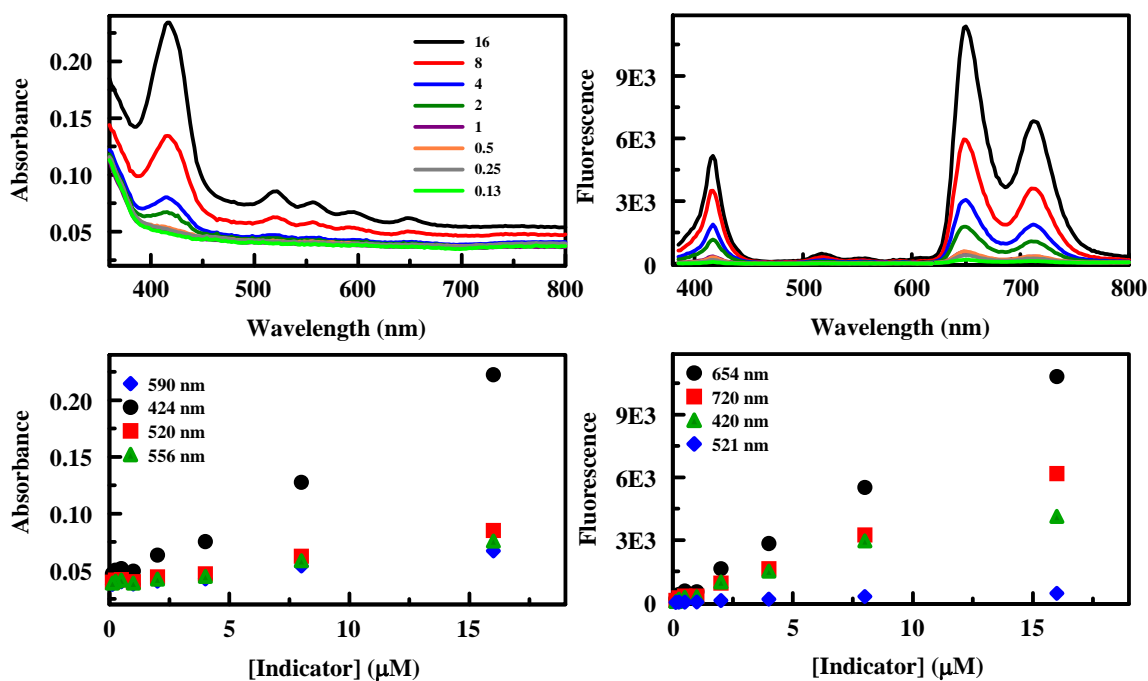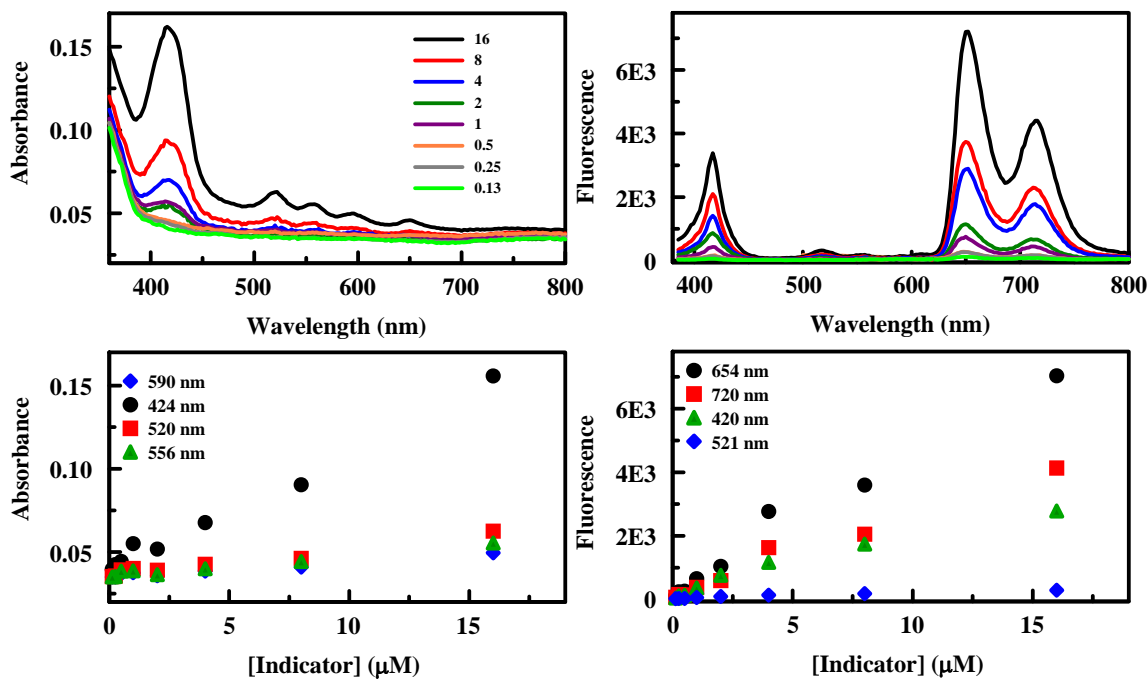
Figure B5. Interaction of C14-GMBS-Indol with *E. coli*. Absorbance (left) and fluorescence (right) spectra for C_1S_3-Indol (16 µM) in the presence and absence (black) of bacterial cells (concentrations in cells/mL provided in the legend). All solutions contain 15% DMSO.
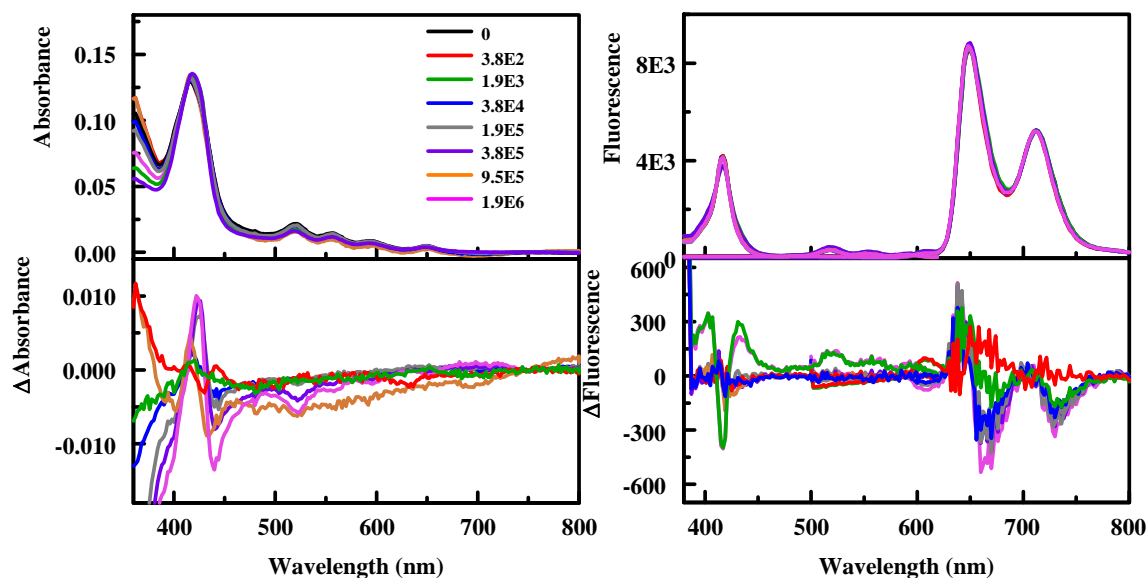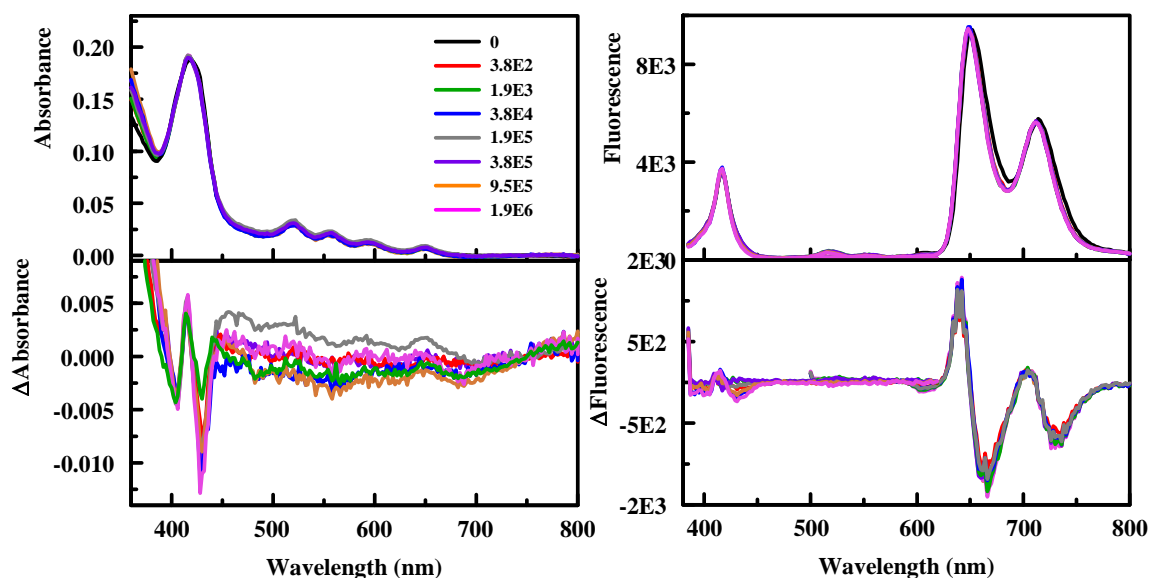

Figure B6. Interaction of C14-GMBS-Indol with *B. cereus*. Absorbance (left) and fluorescence (right) spectra for C_1S_3-Indol (16 µM) in the presence and absence (black) of bacterial cells (concentrations in cells/mL provided in the legend). All solutions contain 15% DMSO.
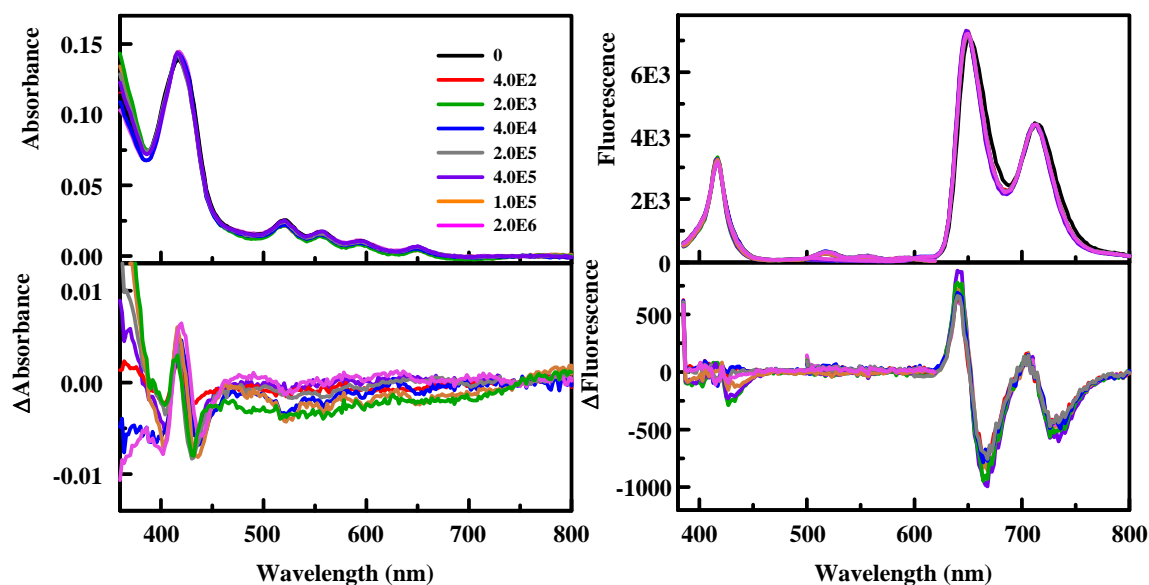
Figure B7. C14-EMCS-Indol. Absorbance (left) and fluorescence (right) characteristics for the EMCS crosslinked C_1S_3TPP modified C14-Indol. All spectra were collected in 15% DMSO. Tracer concentrations are provided in the legend (µM).
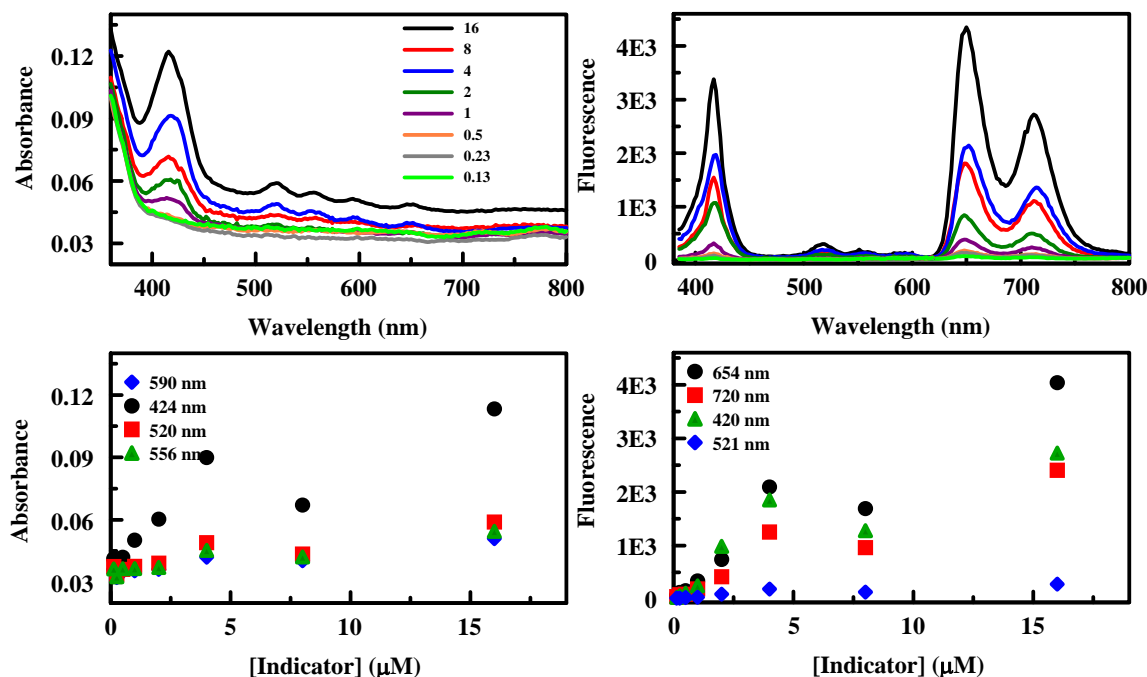

Figure B8. Interaction of C14-EMCS-Indol with *E. coli*. Absorbance (left) and fluorescence (right) spectra for C_1S_3-Indol (16 µM) in the presence and absence (black) of bacterial cells (concentrations in cells/mL provided in the legend). All solutions contain 15% DMSO.

Figure B9. Interaction of C14-EMCS-Indol with *B. cereus*. Absorbance (left) and fluorescence (right) spectra for C_1S_3-Indol (16 µM) in the presence and absence (black) of bacterial cells (concentrations in cells/mL provided in the legend). All solutions contain 15% DMSO.
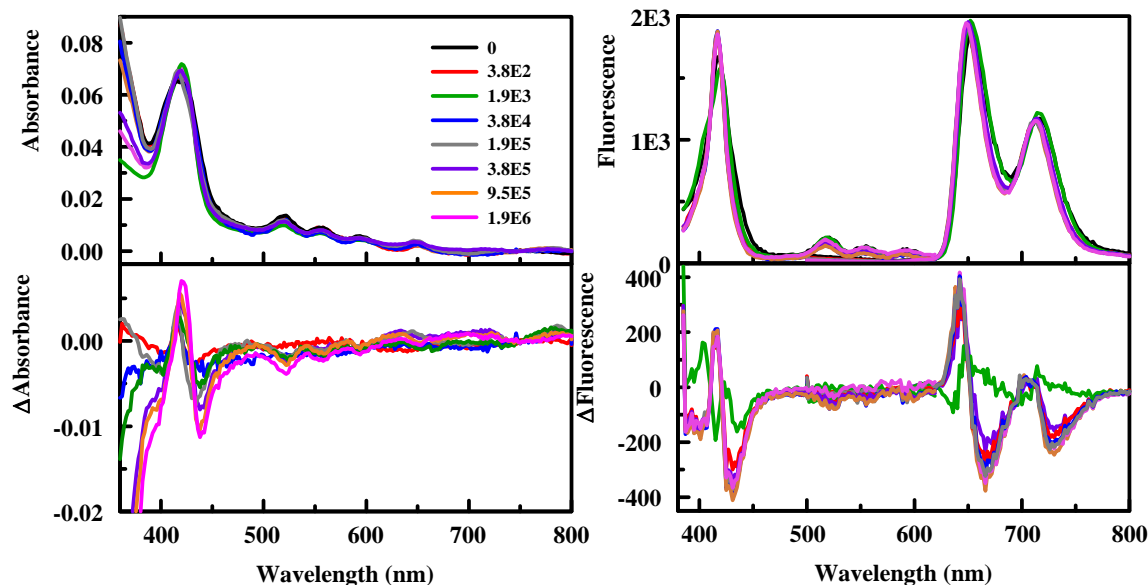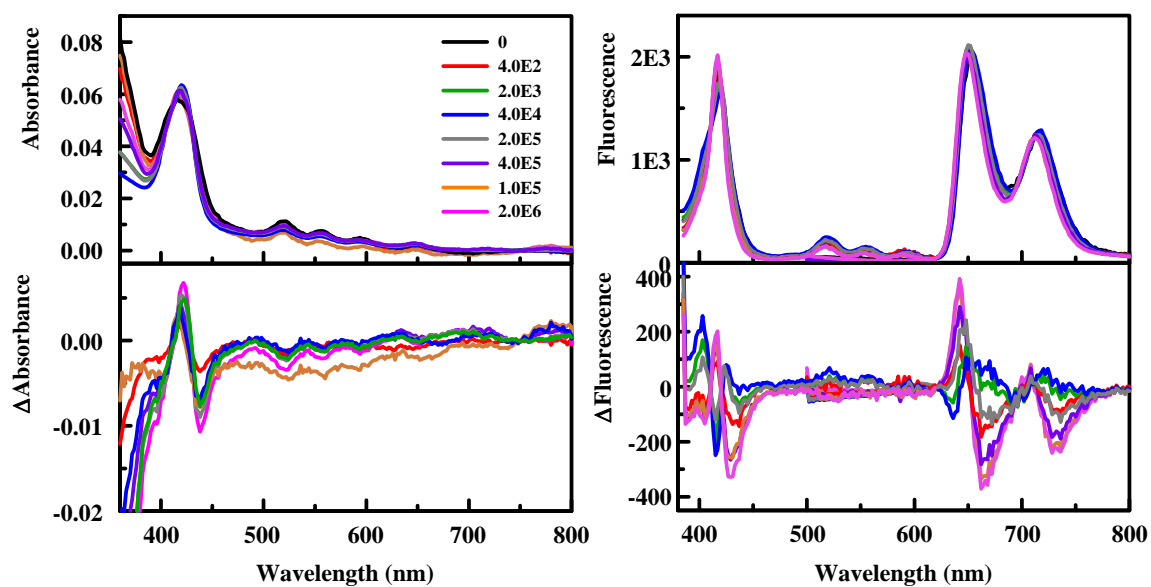

Figure B10. C14-MBS-Indol. Absorbance (left) and fluorescence (right) characteristics for the MBS crosslinked C_1S_3TPP modified C14-Indol. All spectra were collected in 15% DMSO. Tracer concentrations are provided in the legend (µM).

Figure B11. Interaction of C14-MBS-Indol with *E. coli*. Absorbance (left) and fluorescence (right) spectra for C_1S_3-Indol (16 μM) in the presence and absence (black) of bacterial cells (concentrations in cells/mL provided in the legend). All solutions contain 15% DMSO.

Figure B12. Interaction of C14-MBS-Indol with *B. cereus*. Absorbance (left) and fluorescence (right) spectra for C_1S_3-Indol (16 μM) in the presence and absence (black) of bacterial cells (concentrations in cells/mL provided in the legend). All solutions contain 15% DMSO.

Figure B13. C14-SMCC-Indol. Absorbance (left) and fluorescence (right) characteristics for the SMCC crosslinked C_1S_3TPP modified C14-Indol. All spectra were collected in 15% DMSO. Tracer concentrations are provided in the legend (μM).
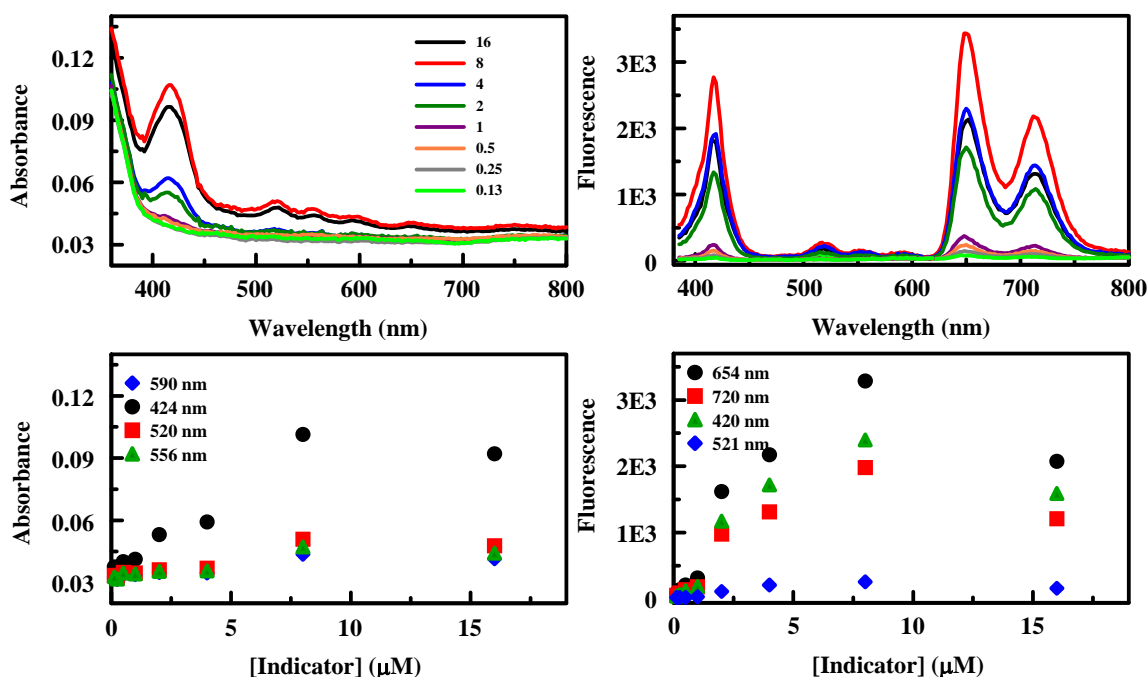

Figure B14. Interaction of C14-MBS-Indol with *E. coli*. Absorbance (left) and fluorescence (right) spectra for C_1S_3-Indol (16 μM) in the presence and absence (black) of bacterial cells (concentrations in cells/mL provided in the legend). All solutions contain 15% DMSO.
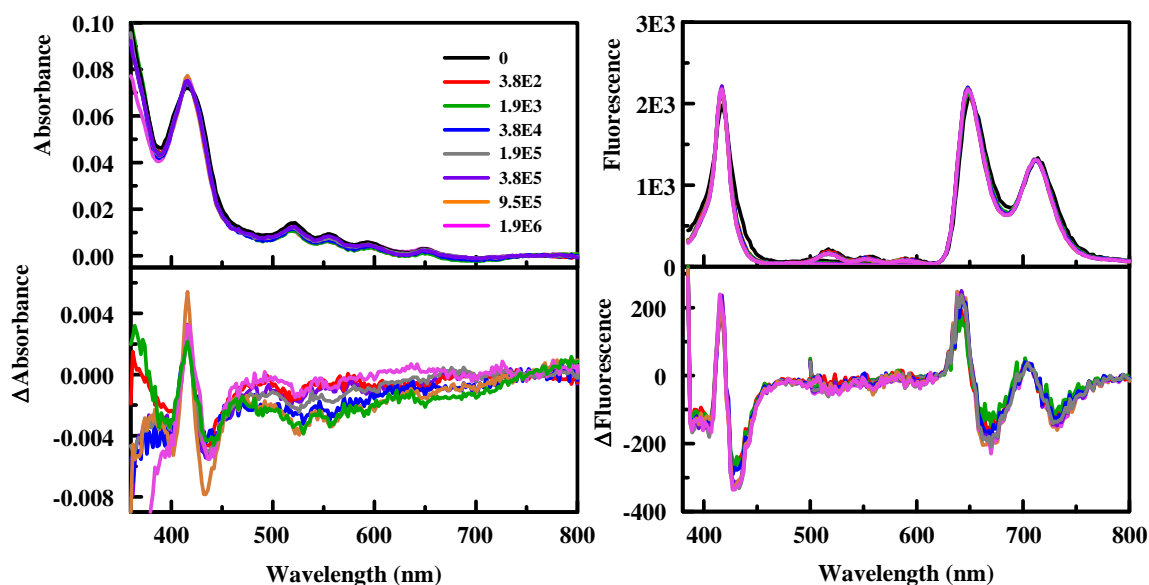
Figure B15. Interaction of C14-MBS-Indol with *B. cereus*. Absorbance (left) and fluorescence (right) spectra for C_1S_3-Indol (16 µM) in the presence and absence (black) of bacterial cells (concentrations in cells/mL provided in the legend). All solutions contain 15% DMSO.
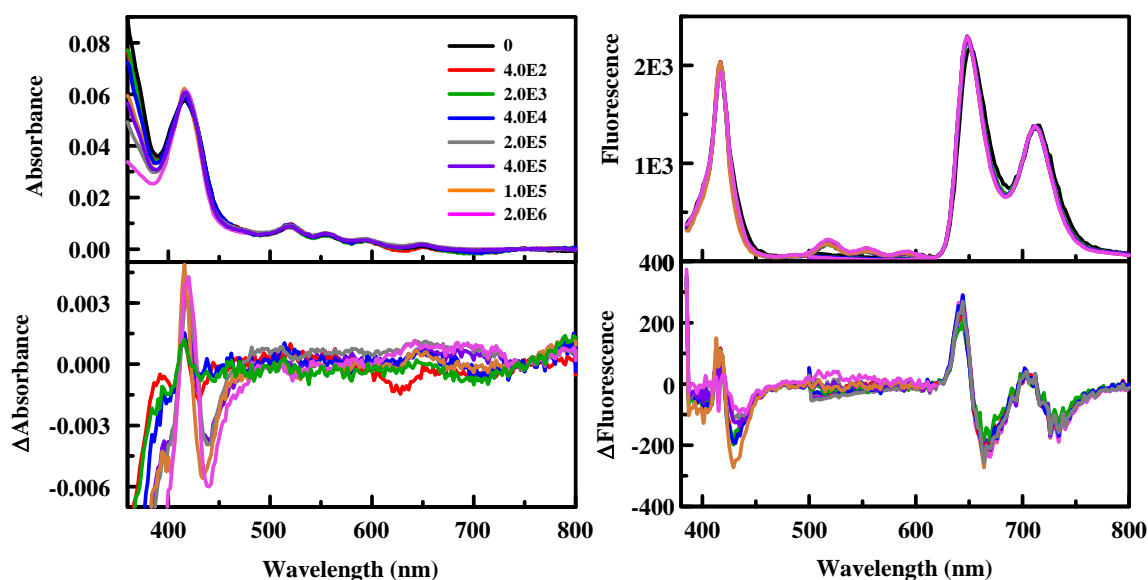
APPENDIX C

C1-INDOL CROSSLINKED C$_1$S$_3$TPP CONSTRUCTS

Figure C1. C1-AMAS-Indol. Absorbance (left) and fluorescence (right) characteristics for the AMAS crosslinked C_1S_3TPP modified C1-Indol. All spectra were collected in 15% DMSO. Tracer concentrations are provided in the legend (μM).
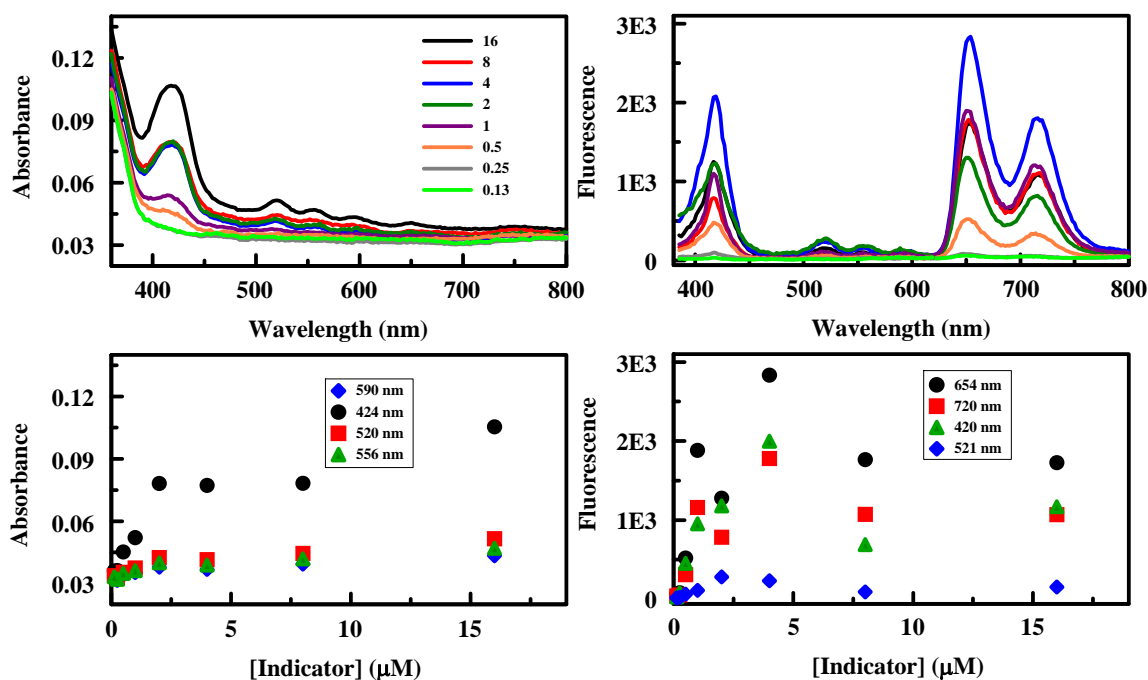

Figure C2. Interaction of C1-AMAS-Indol with *E. coli*. Absorbance (left) and fluorescence (right) spectra for C_1S_3-Indol (16 μM) in the presence and absence (black) of bacterial cells (concentrations in cells/mL provided in the legend). All solutions contain 15% DMSO.
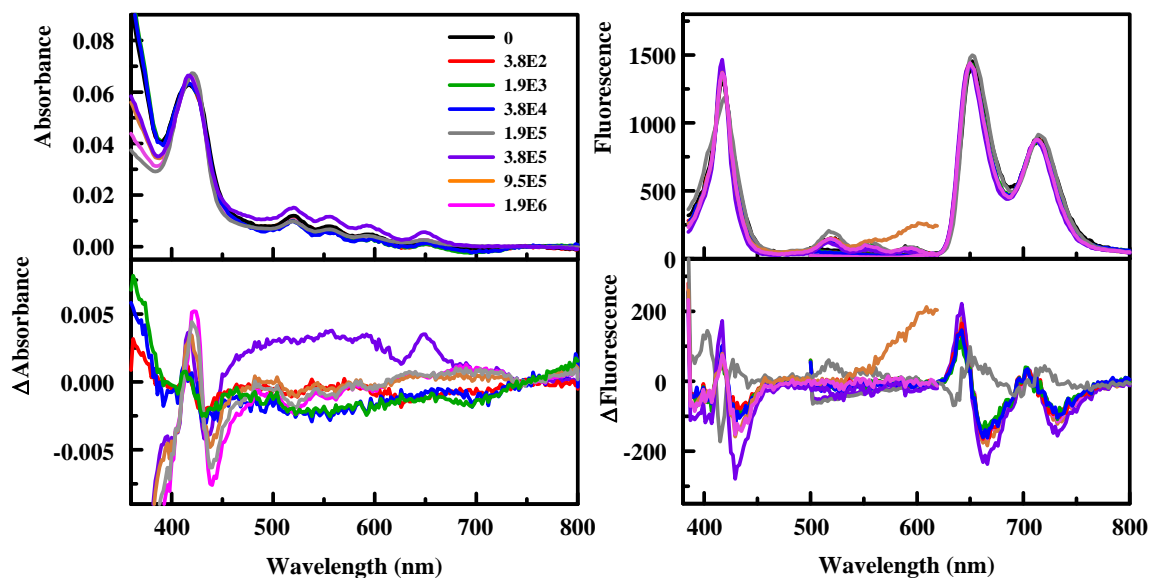
Figure C3. Interaction of C1-AMAS-Indol with *B. cereus*. Absorbance (left) and fluorescence (right) spectra for C_1S_3-Indol (16 μM) in the presence and absence (black) of bacterial cells (concentrations in cells/mL provided in the legend). All solutions contain 15% DMSO.
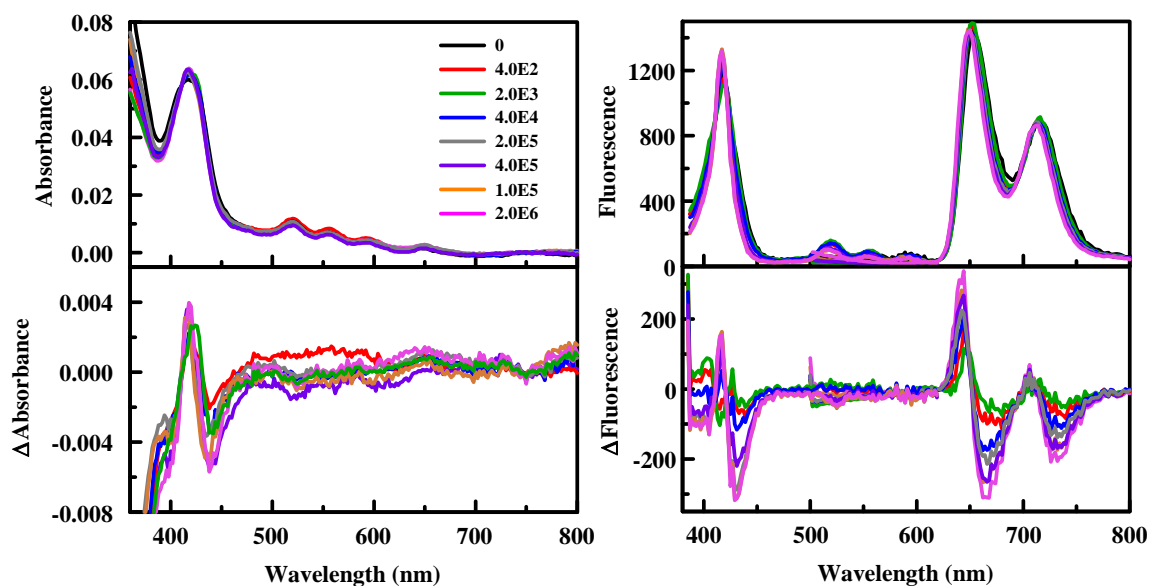

Figure C4. C1-GMBS-Indol. Absorbance (left) and fluorescence (right) characteristics for the EMBS crosslinked C_1S_3TPP modified C1-Indol. All spectra were collected in 15% DMSO. Tracer concentrations are provided in the legend (μM).
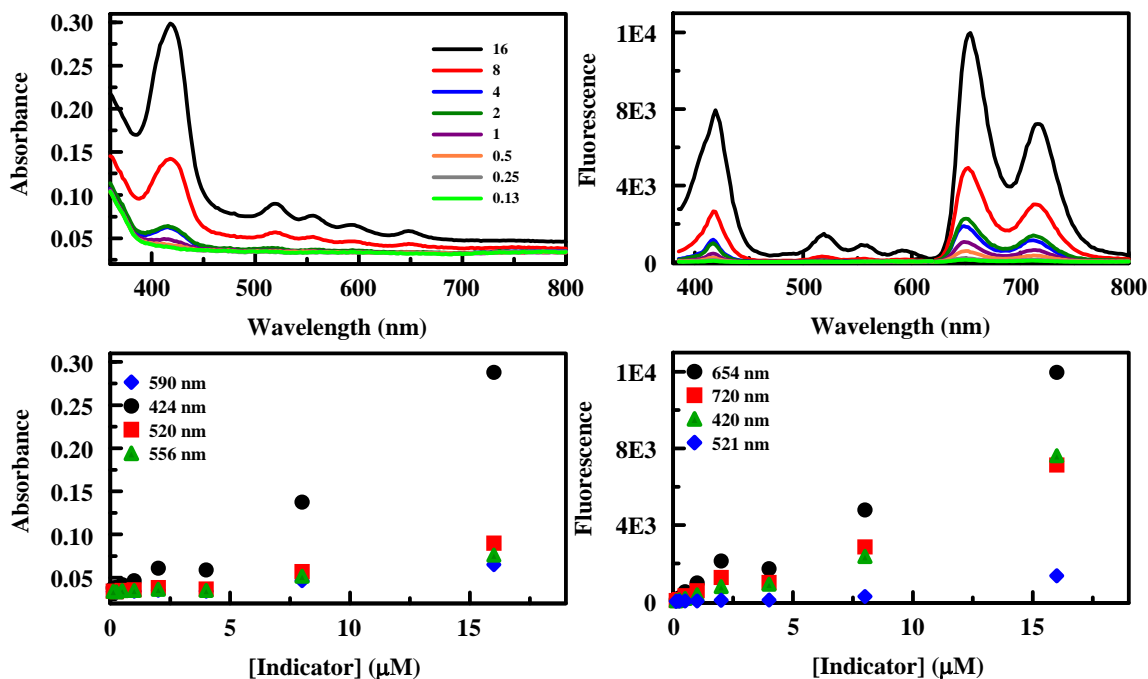
Figure C5. Interaction of C1-GMBS-Indol with *E. coli*. Absorbance (left) and fluorescence (right) spectra for C_1S_3-Indol (16 µM) in the presence and absence (black) of bacterial cells (concentrations in cells/mL provided in the legend). All solutions contain 15% DMSO.

Figure C6. Interaction of C1-GMBS-Indol with *B. cereus*. Absorbance (left) and fluorescence (right) spectra for C_1S_3-Indol (16 µM) in the presence and absence (black) of bacterial cells (concentrations in cells/mL provided in the legend). All solutions contain 15% DMSO.
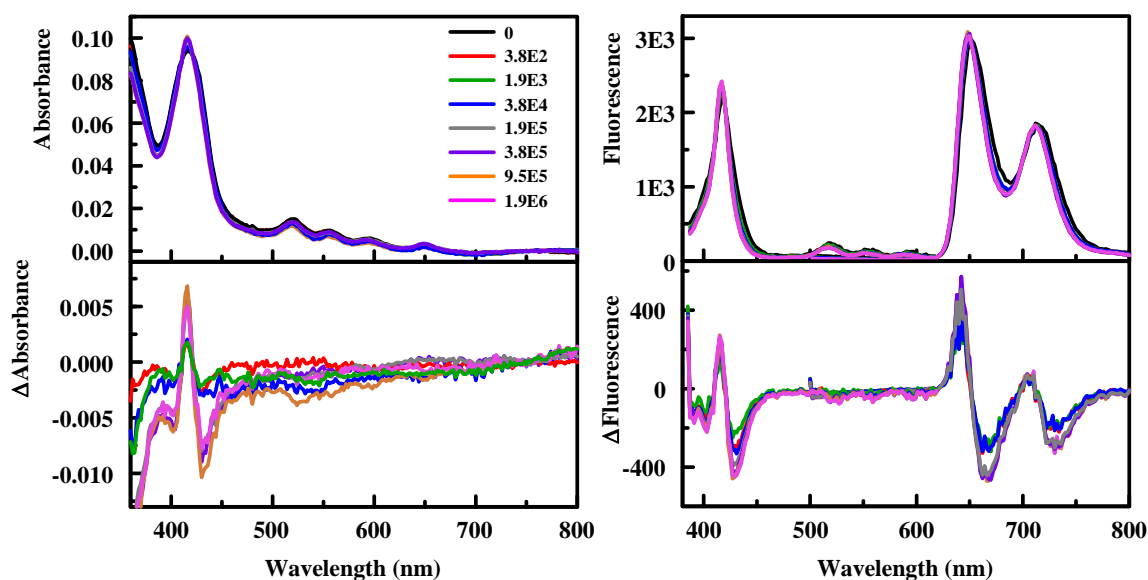
Figure C7. C1-EMCS-Indol. Absorbance (left) and fluorescence (right) characteristics for the EMCS crosslinked C_1S_3TPP modified C1-Indol. All spectra were collected in 15% DMSO. Tracer concentrations are provided in the legend (μM).

Figure C8. Interaction of C1-EMCS-Indol with *E. coli*. Absorbance (left) and fluorescence (right) spectra for C_1S_3-Indol (16 μM) in the presence and absence (black) of bacterial cells (concentrations in cells/mL provided in the legend). All solutions contain 15% DMSO.
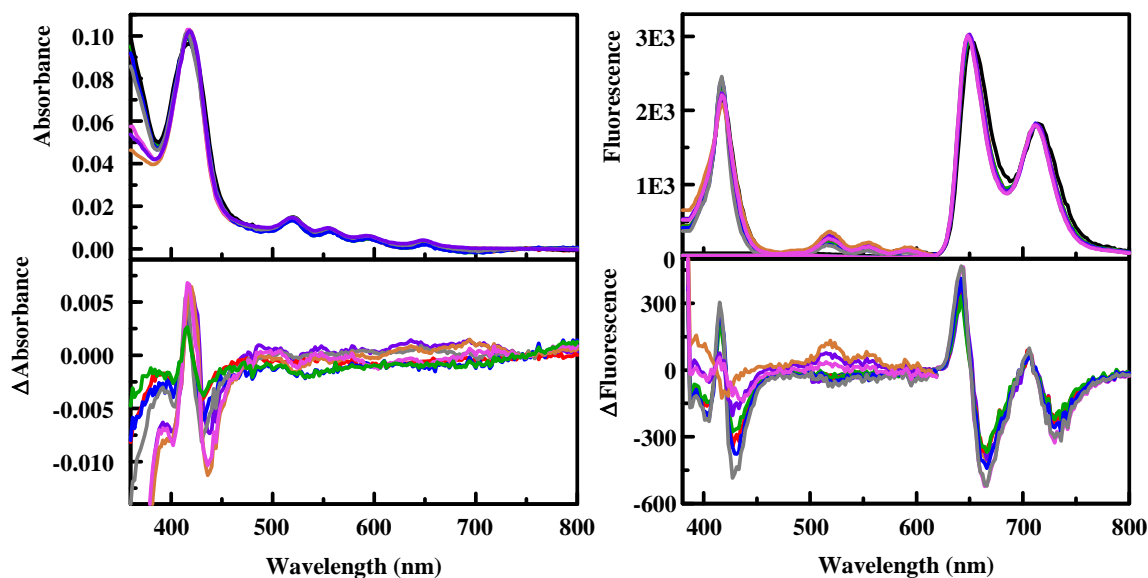
Figure C9. Interaction of C1-EMCS-Indol with *B. cereus*. Absorbance (left) and fluorescence (right) spectra for C_1S_3-Indol (16 µM) in the presence and absence (black) of bacterial cells (concentrations in cells/mL provided in the legend). All solutions contain 15% DMSO.

Figure C10. C1-MBS-Indol. Absorbance (left) and fluorescence (right) characteristics for the MBS crosslinked C_1S_3TPP modified C1-Indol. All spectra were collected in 15% DMSO. Tracer concentrations are provided in the legend (µM).
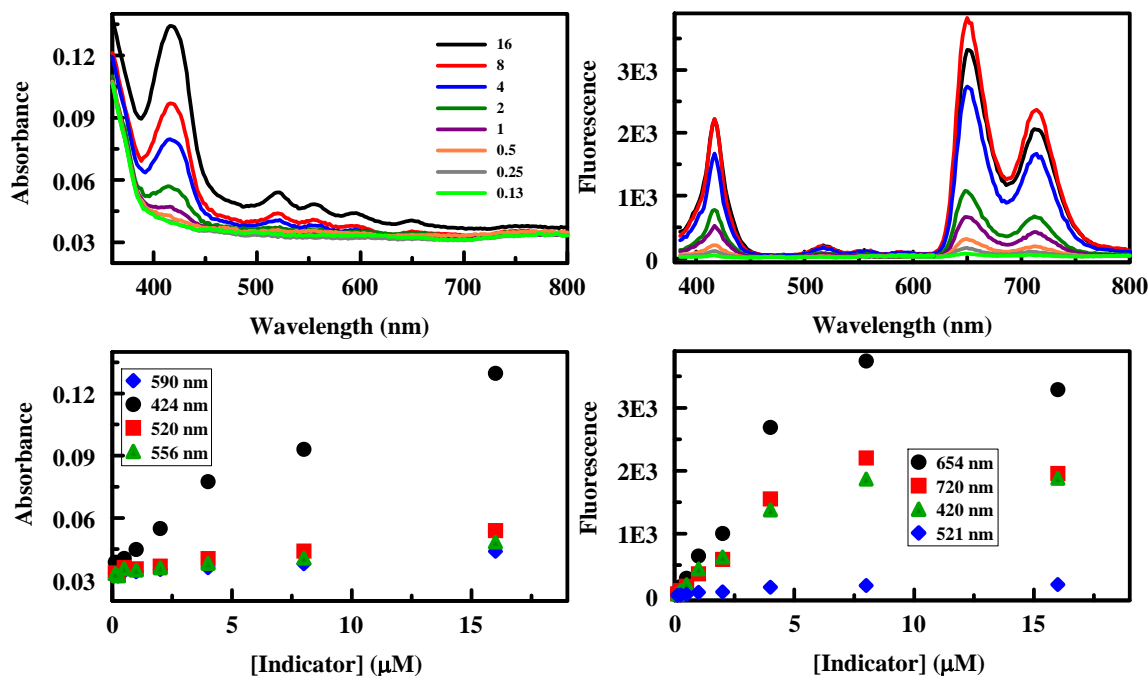
Figure C11. Interaction of C1-MBS-Indol with *E. coli*. Absorbance (left) and fluorescence (right) spectra for C_1S_3-Indol (16 μM) in the presence and absence (black) of bacterial cells (concentrations in cells/mL provided in the legend). All solutions contain 15% DMSO.
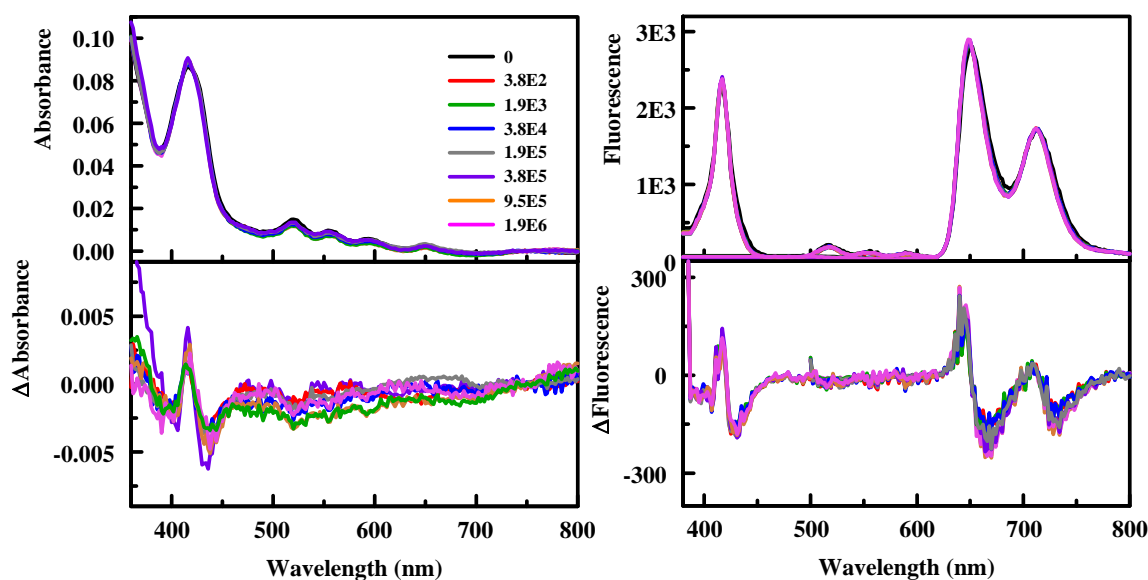

Figure C12. Interaction of C1-MBS-Indol with *B. cereus*. Absorbance (left) and fluorescence (right) spectra for C_1S_3-Indol (16 μM) in the presence and absence (black) of bacterial cells (concentrations in cells/mL provided in the legend). All solutions contain 15% DMSO.
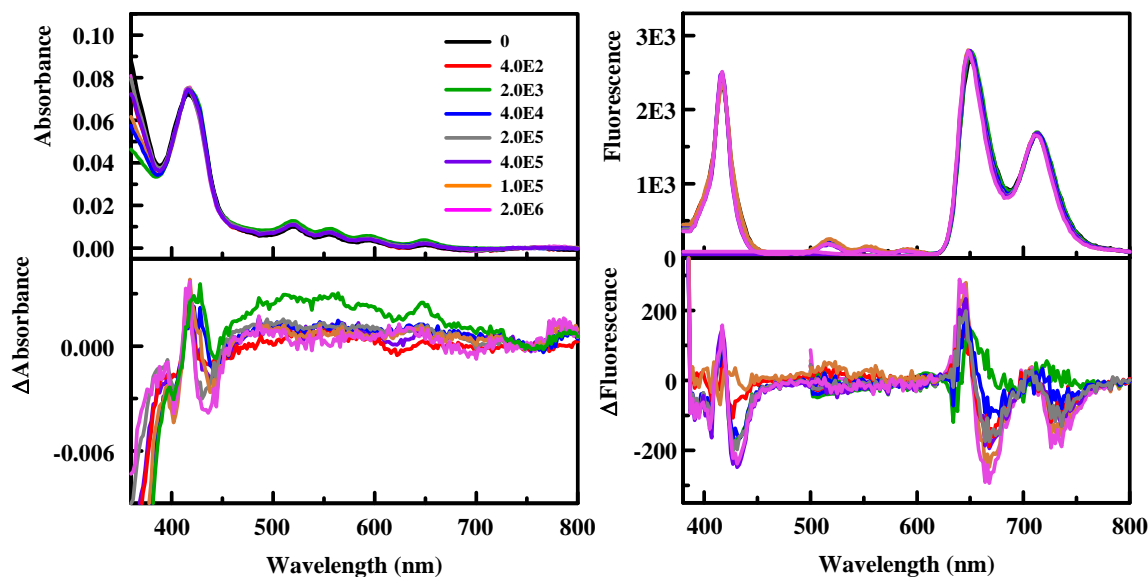
Figure C13. C1-SMCC-Indol. Absorbance (left) and fluorescence (right) characteristics for the SMCC crosslinked C_1S_3TPP modified C1-Indol. All spectra were collected in 15% DMSO. Tracer concentrations are provided in the legend (μM).
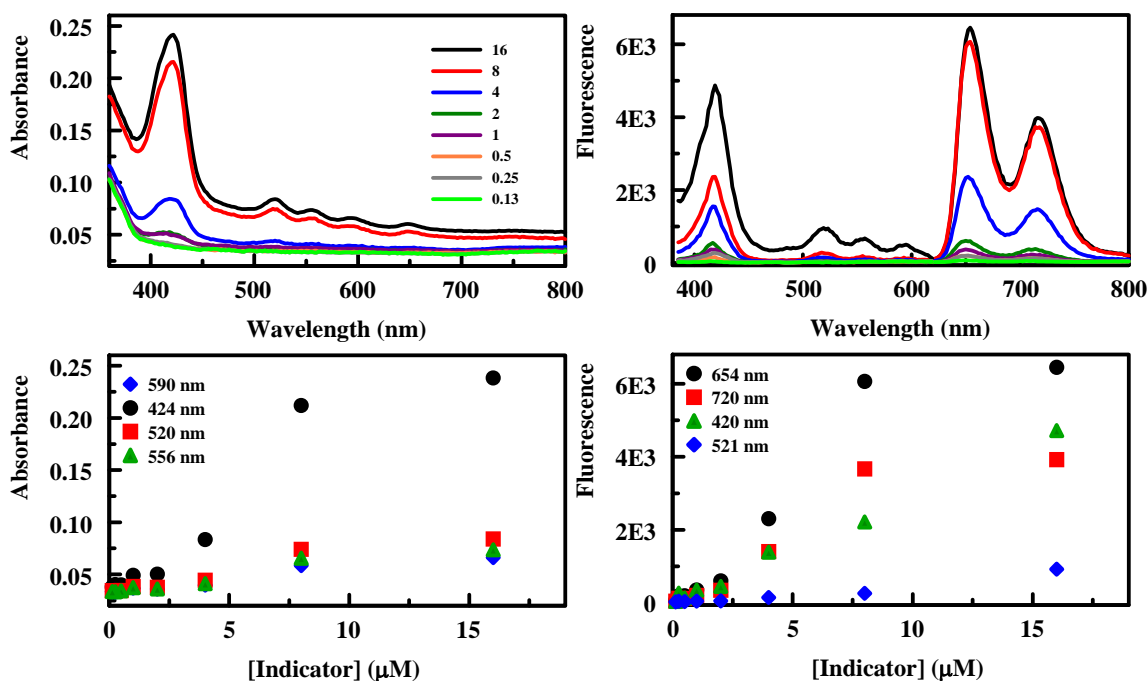

Figure C14. Interaction of C1-SMCC-Indol with *E. coli*. Absorbance (left) and fluorescence (right) spectra for C_1S_3-Indol (16 μM) in the presence and absence (black) of bacterial cells (concentrations in cells/mL provided in the legend). All solutions contain 15% DMSO.
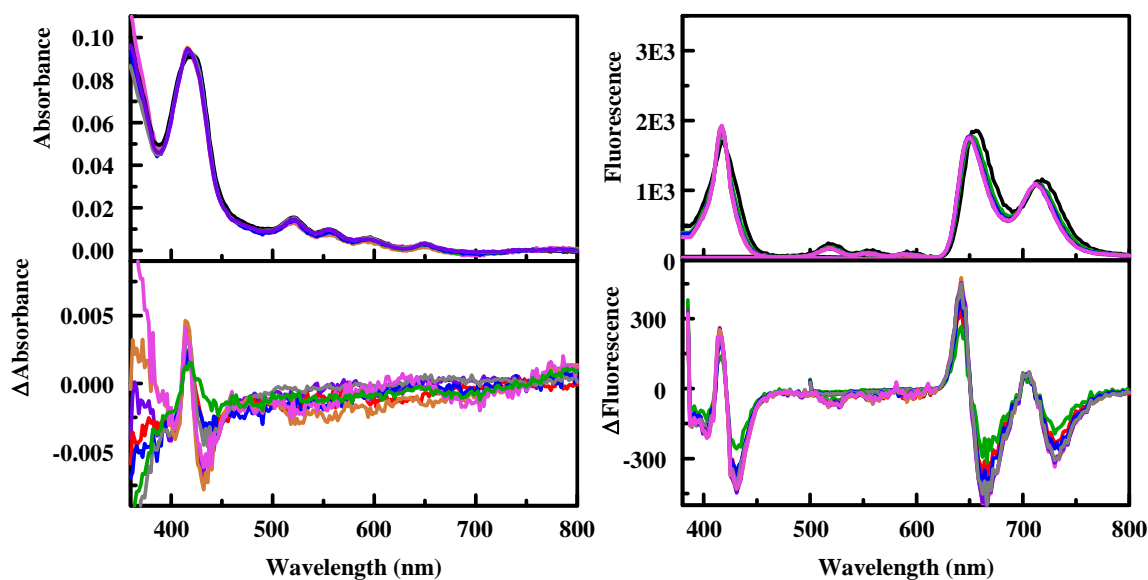
Figure C15. Interaction of C1-SMCC-Indol with *B. cereus*. Absorbance (left) and fluorescence (right) spectra for C_1S_3-Indol (16 μM) in the presence and absence (black) of bacterial cells (concentrations in cells/mL provided in the legend). All solutions contain 15% DMSO.